Satellite Time-Series Analysis. Combined InSAR/SAR-Amplitude-based Approaches for Change Detection Analyses

Antonio Pepe

Istituto per il Rilevamento Elettromagnetico dell'Ambiente (IREA)
Consiglio Nazionale delle Ricerche (CNR)
Via Diocleziano, 328, 80124 Napoli (Italy)

Non-Local Denoising Filters: Key idea

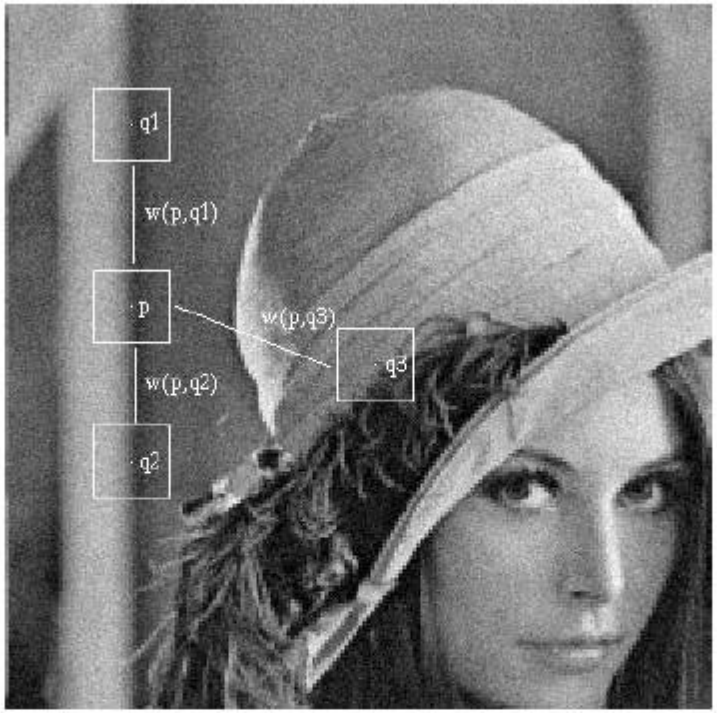

$$NL[v](i) = \sum_{j \in I} w(i,j) v(j),$$

$$w(i,j) = \frac{1}{Z(i)} e^{-\frac{||v(\mathcal{N}_i) - v(\mathcal{N}_j)||_{2,a}^2}{h^2}},$$

$$Z(i) = \sum_j e^{-\frac{||v(\mathcal{N}_i) - v(\mathcal{N}_i)||_{2,a}^2}{h^2}}$$

Figure 1. Scheme of NL-means strategy. Similar pixel neighborhoods give a large weight, w(p,q1) and w(p,q2), while much different neighborhoods give a small weight w(p,q3).

Multi-Temporal Non-Local Filters

PATCHES ARE EXTRACTED FROM A SEQUENCE OF N SAR IMAGES

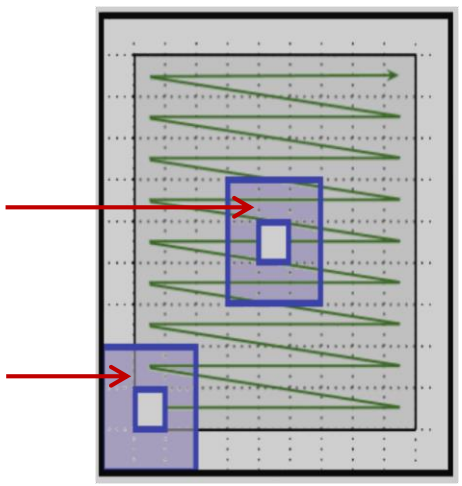

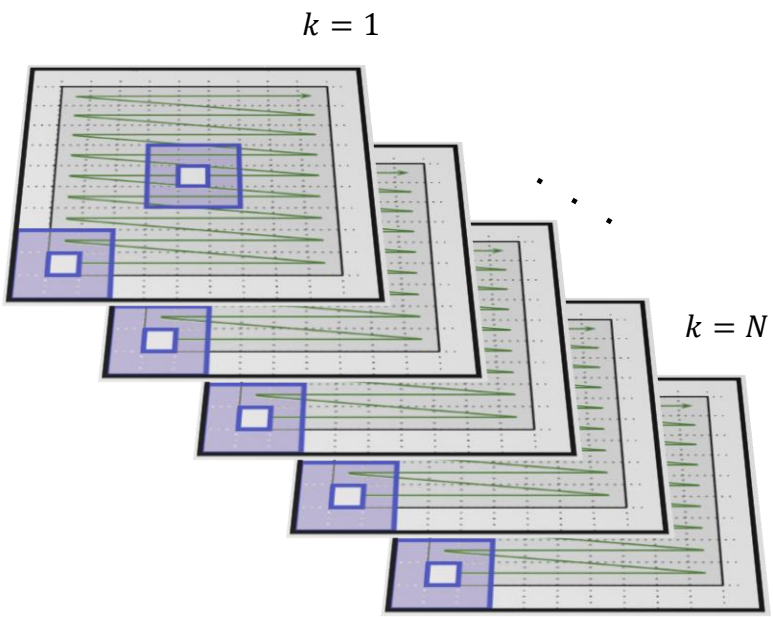

Experiments in India

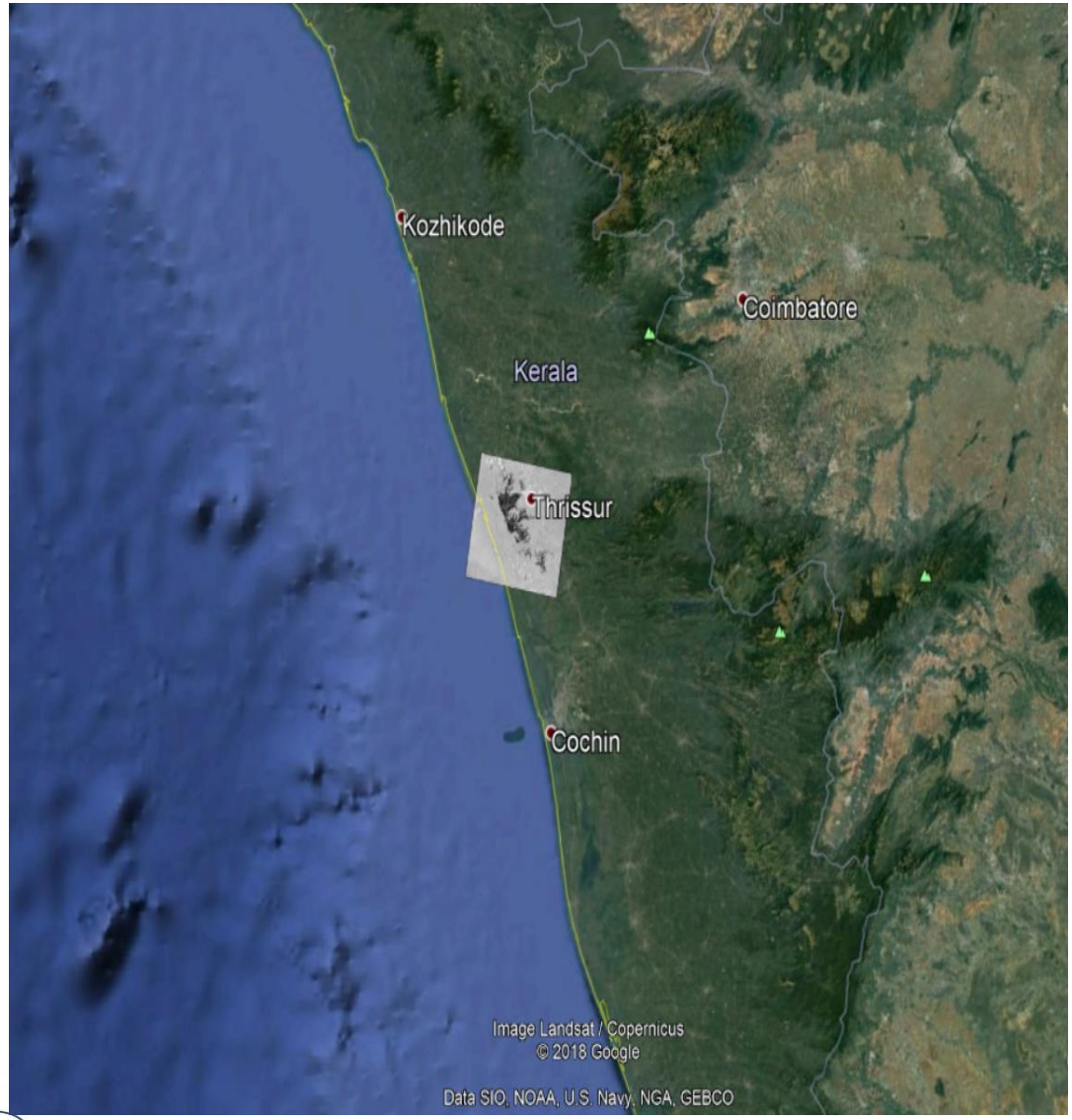

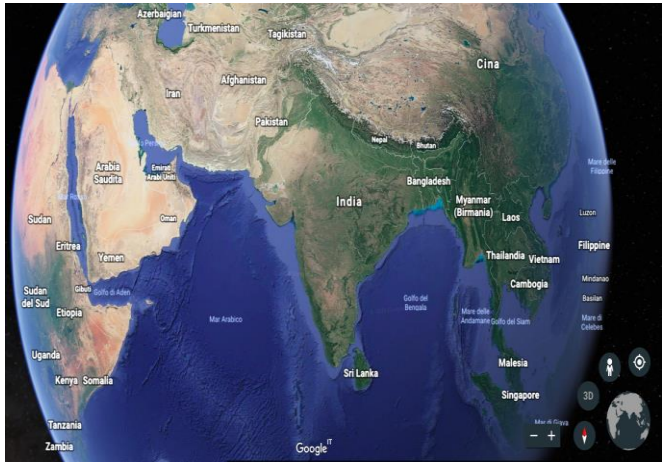

FLOODS IN KERALA REGION

Non-Local Multi-Temporal Filters

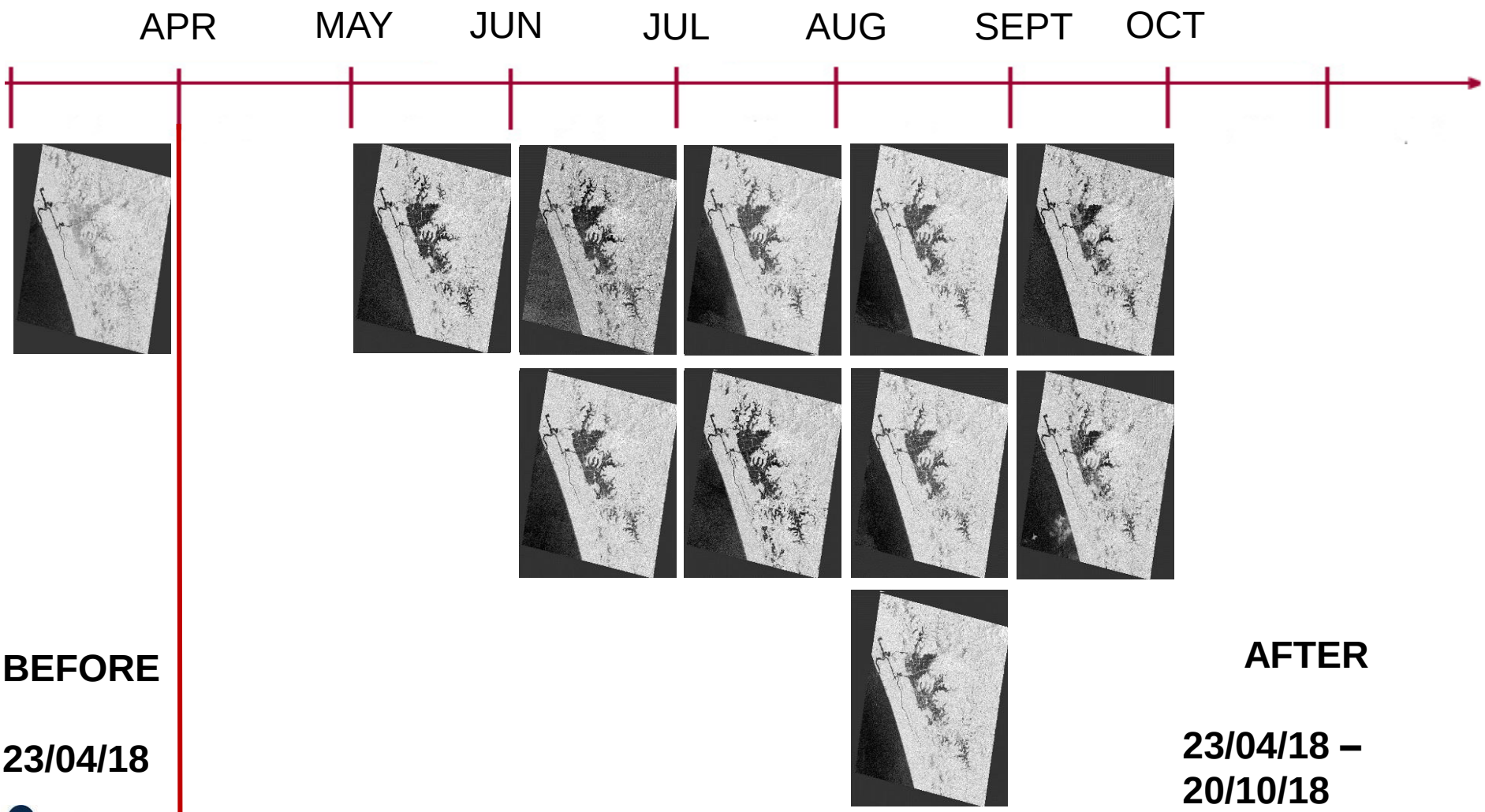

Non-Local Multi-Temporal Filters

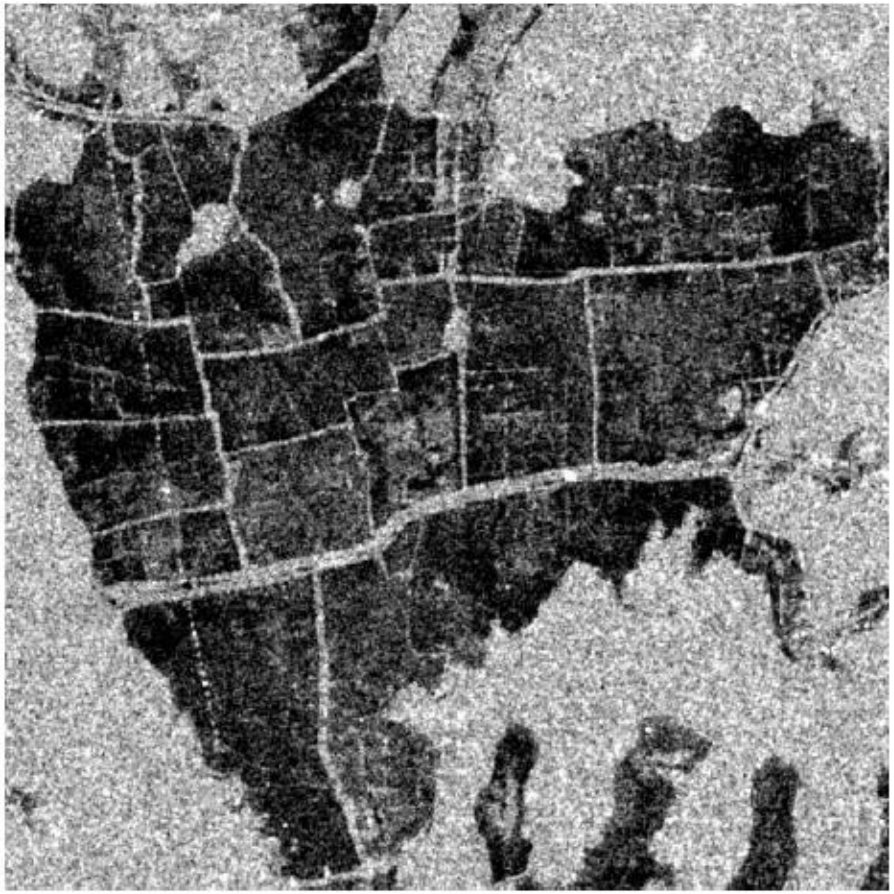

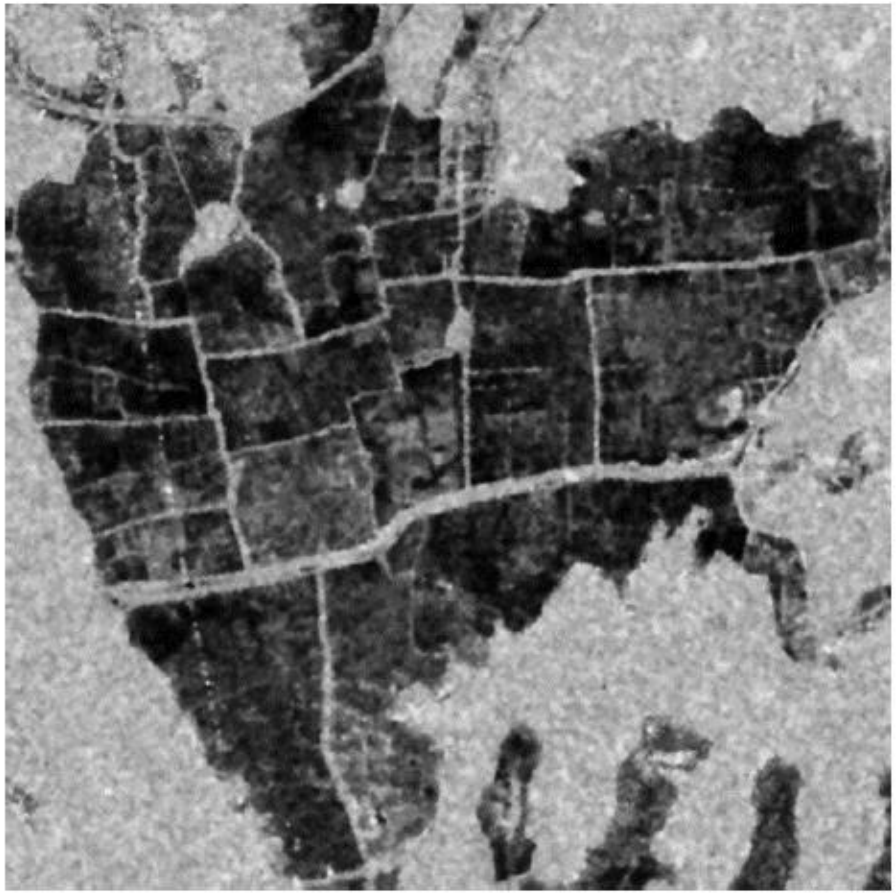

SINGLE **MULTI-TEMPORAL**

InSAR: Basic Principles

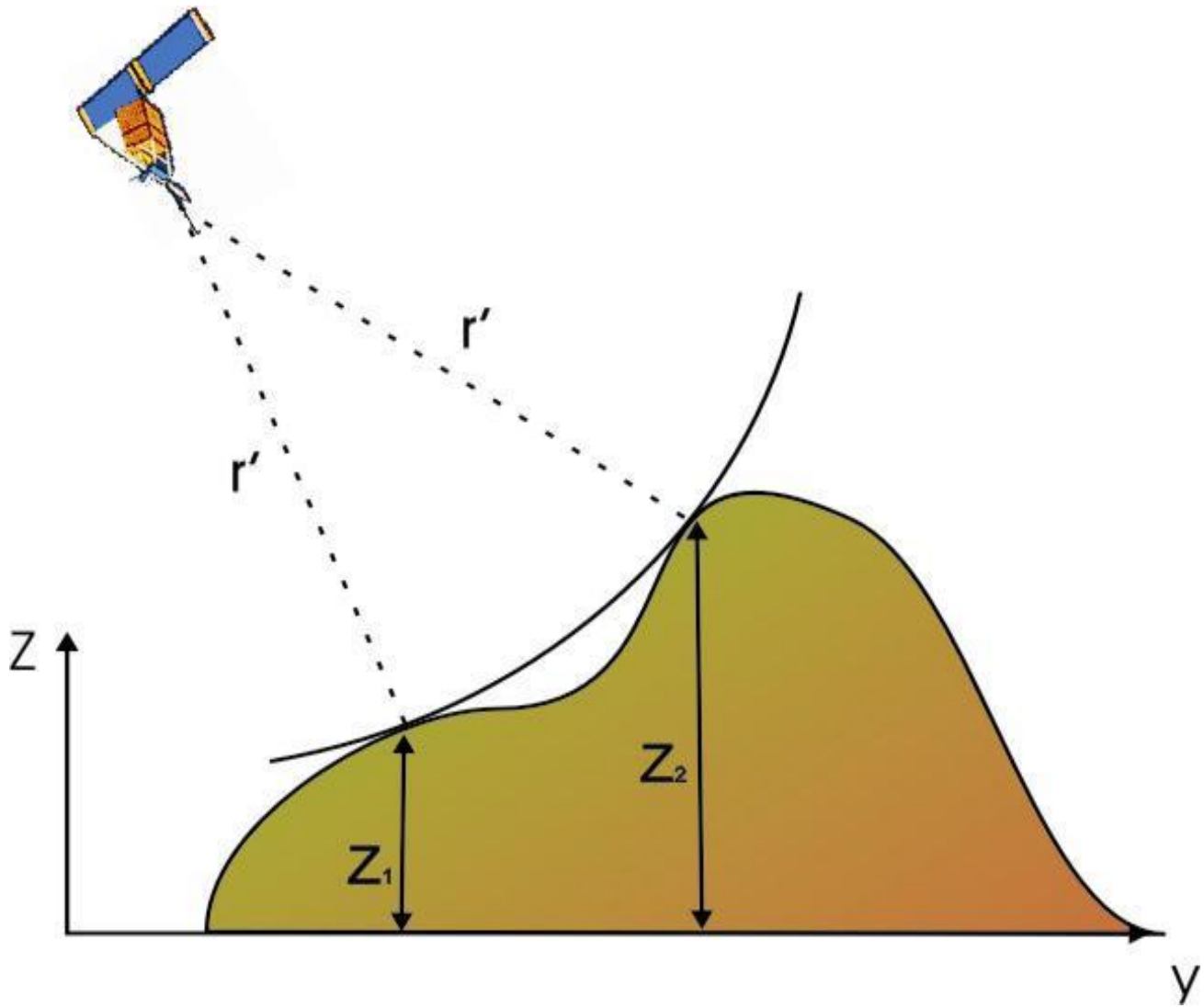

InSAR: Basic Principles

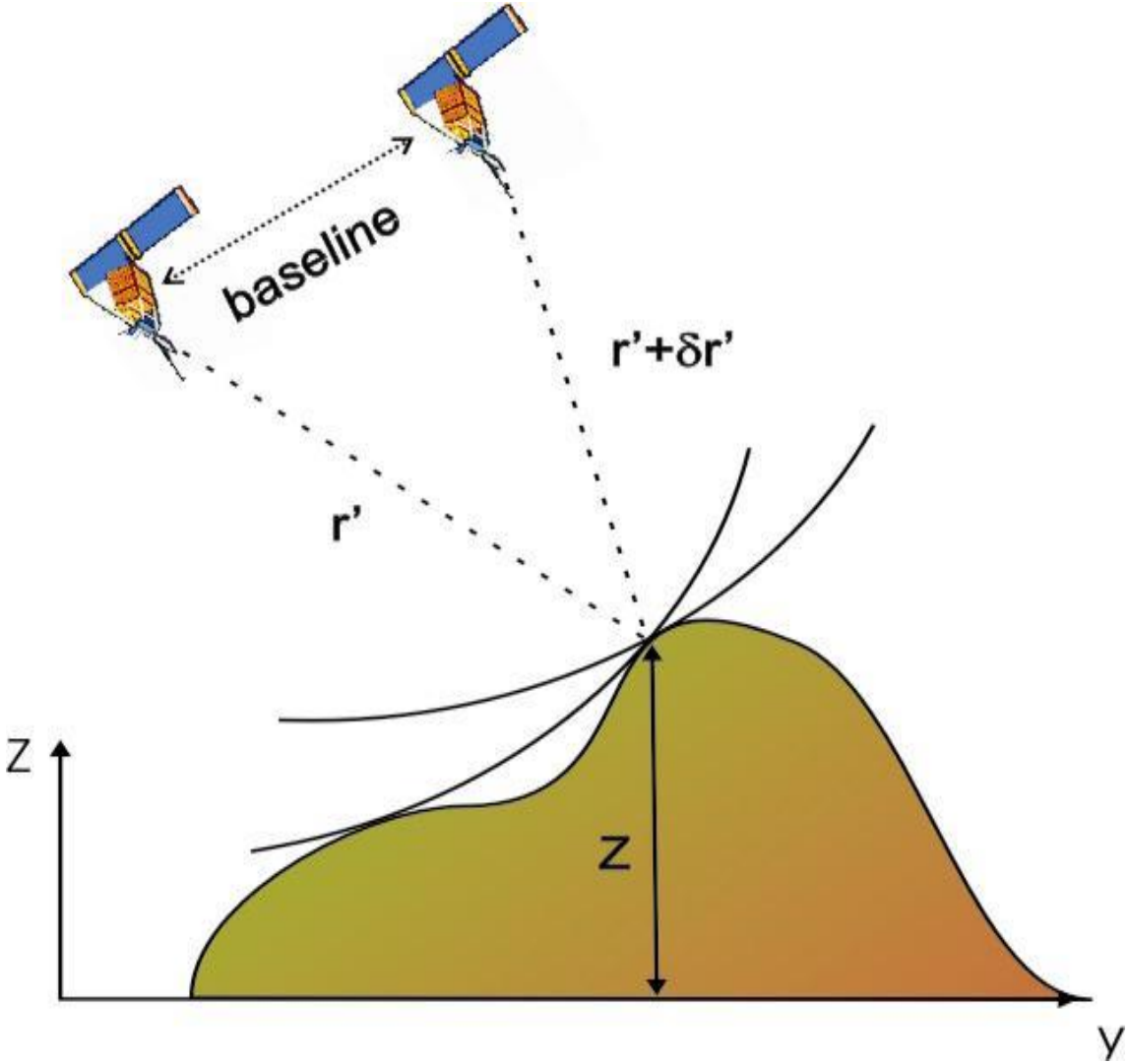

InSAR: Basic Principles

$$\hat{\gamma}_1(x', r') = \gamma(x', r')\exp\left[-j\frac{4\pi}{\lambda}r'\right]$$

$$\updownarrow$$

$$\hat{\gamma}_2(x', r' + \delta r') = \gamma(x', r')\exp\left[-j\frac{4\pi}{\lambda}(r' + \delta r')\right]$$

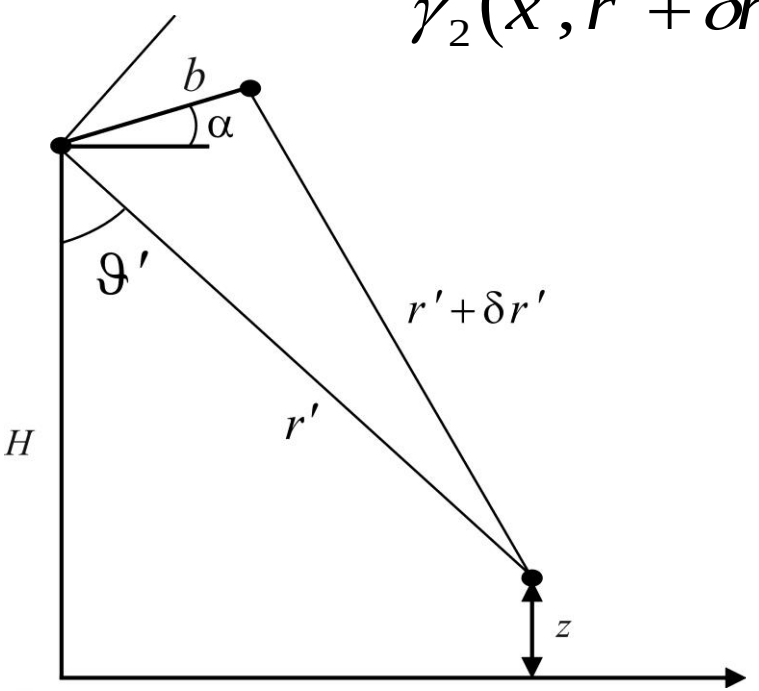

Reflectiviy function

$$\gamma(x', r')$$

InSAR: Basic Principles

$$\hat{\gamma}_1(x', r') = \gamma(x', r')\exp\left[-j\frac{4\pi}{\lambda}r'\right]$$

$$\hat{\gamma}_2(x', r' + \delta r') = \gamma(x', r')\exp\left[-j\frac{4\pi}{\lambda}(r' + \delta r')\right]$$

$$\boxed{\varphi = Arg\left[\hat{\gamma}_1(x', r')\ \hat{\gamma}_2^*(x', r' + \delta r')\right] = -\frac{4\pi}{\lambda}\delta r'}$$

InSAR: Basic Principles

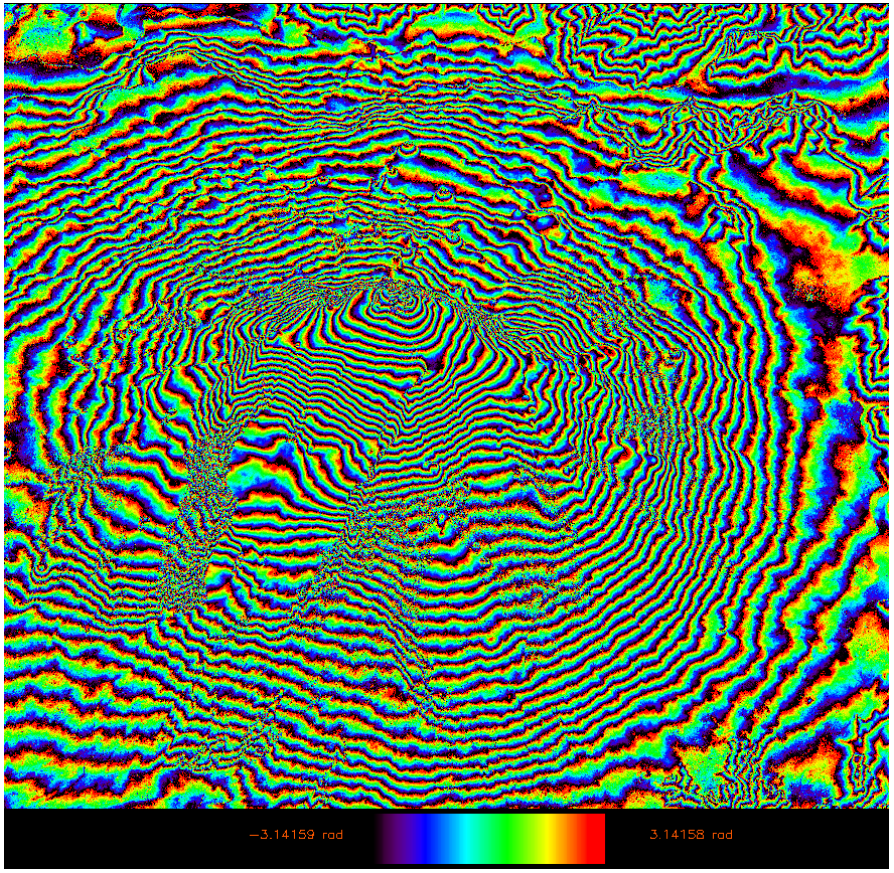

Interferogramma ERS relativo all'Etna.

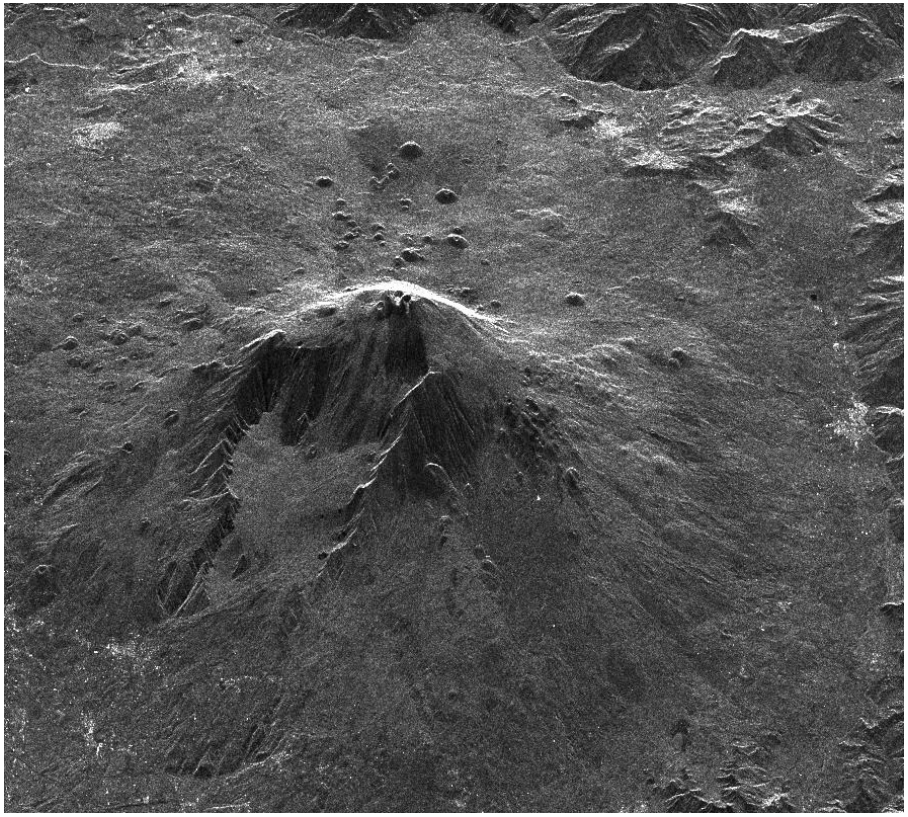

$$\varphi \approx \frac{4\pi}{\lambda} \frac{b_{\perp}}{r' \sin \vartheta'} z$$

Legame (semplificato) fase-quota

Coherence

$$\chi = \frac{\mathrm{E}\left[\hat{\gamma}_1 \hat{\gamma}_2^*\right]}{\sqrt{\mathrm{E}\left[\left|\hat{\gamma}_1\right|^2\right]\mathrm{E}\left[\left|\hat{\gamma}_2\right|^2\right]}} = k \exp\left(j\varphi_0\right)$$

Coherence

ERS Sensor, (1-2 August 1995), area of Napoli Bay.

B_{ort} = 58m

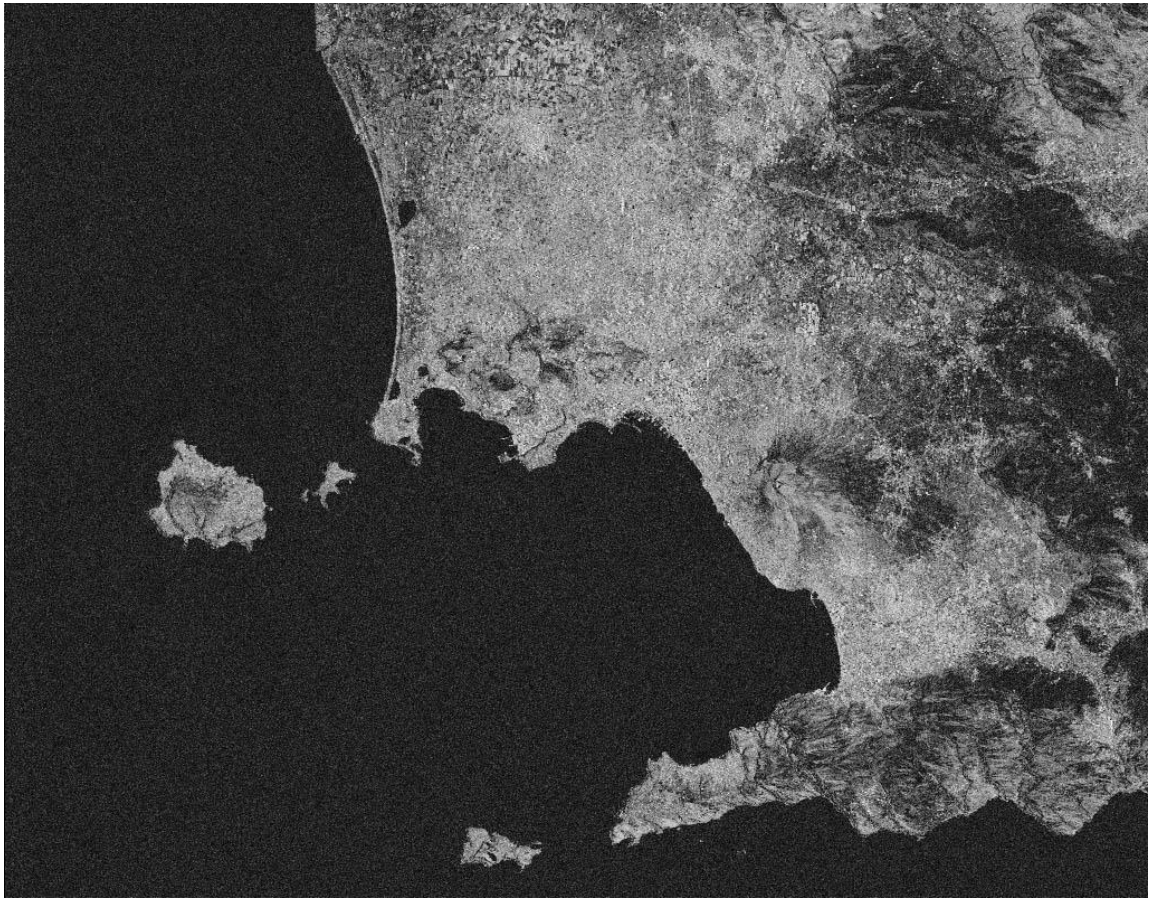

Coherence

ERS InSAR pair (10/01/93-10/10/95) of the Napoli Bay area

B_{ort} = 13m

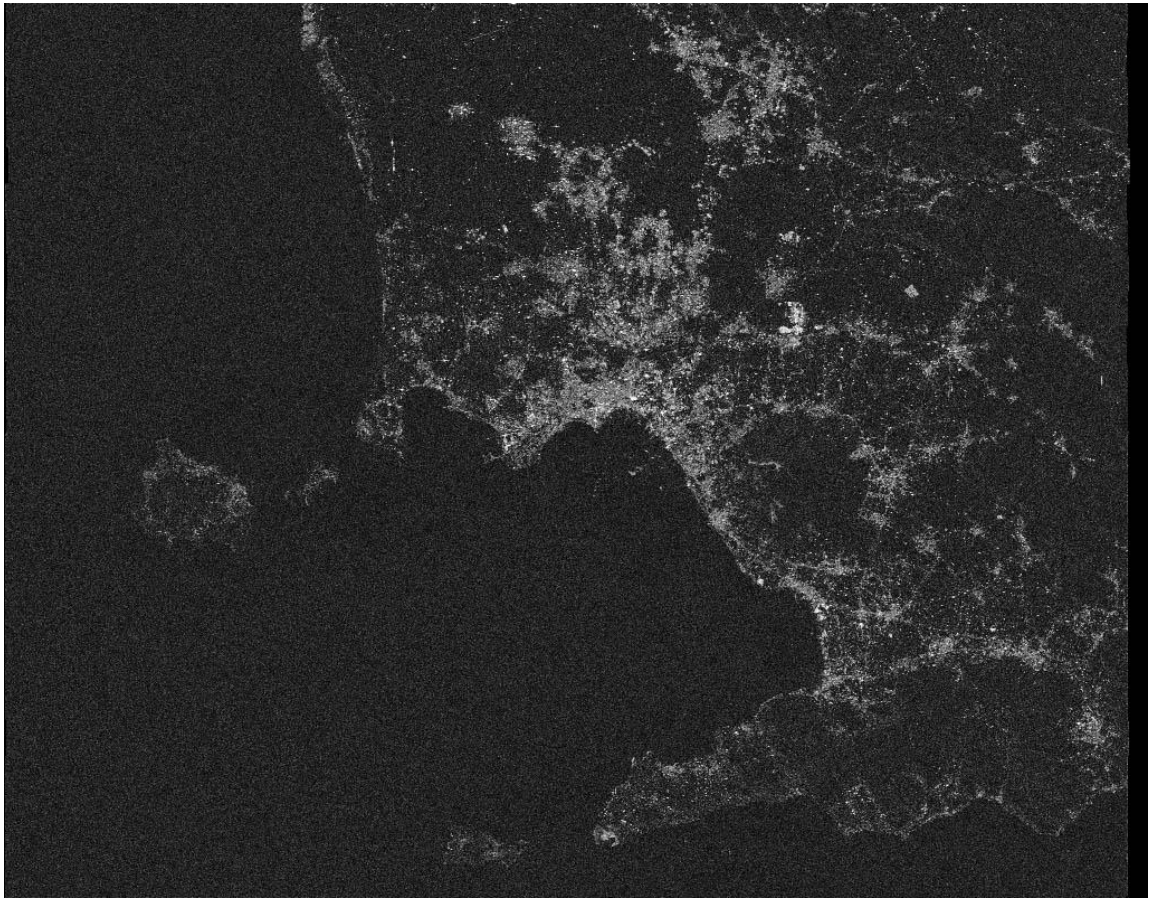

Differential SAR Interferometry (DInSAR)

Different time, same position (**ideal case**) of the two acquisitions

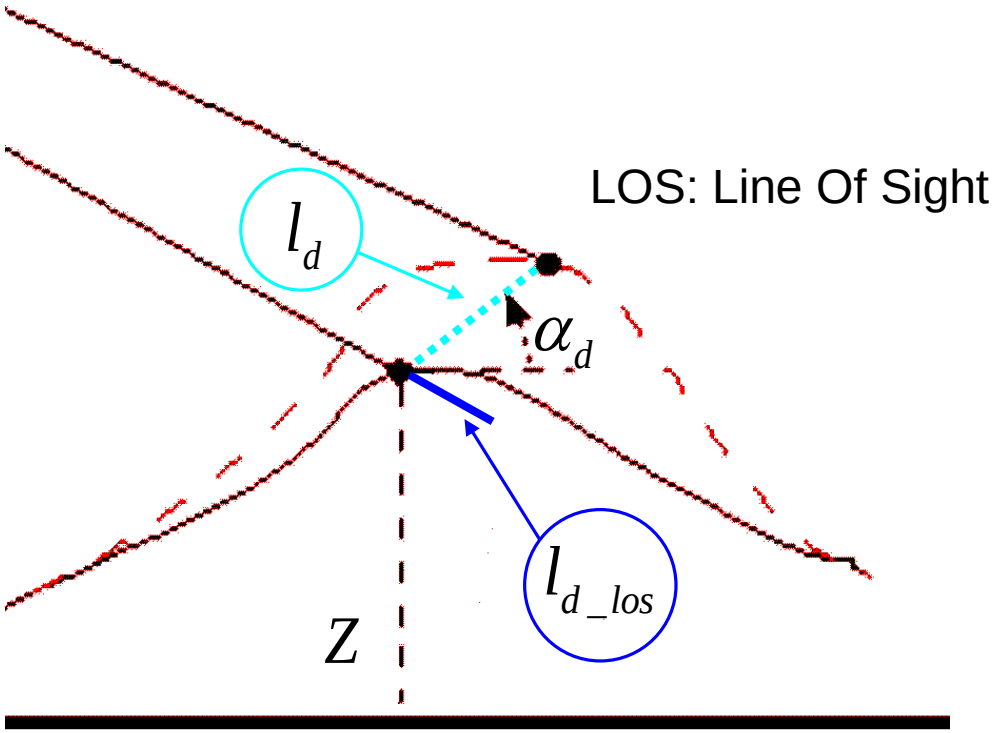

$$\Delta\varphi = \frac{4\pi}{\lambda}\left(r_2 - r_1\right) \approx \frac{4\pi}{\lambda} l_{d_los} = l_d \sin\left(\vartheta' - \alpha_d\right) = \varphi_d$$

Deformation Phase

Mw 7.1 Ridgecrest Earthquake, California

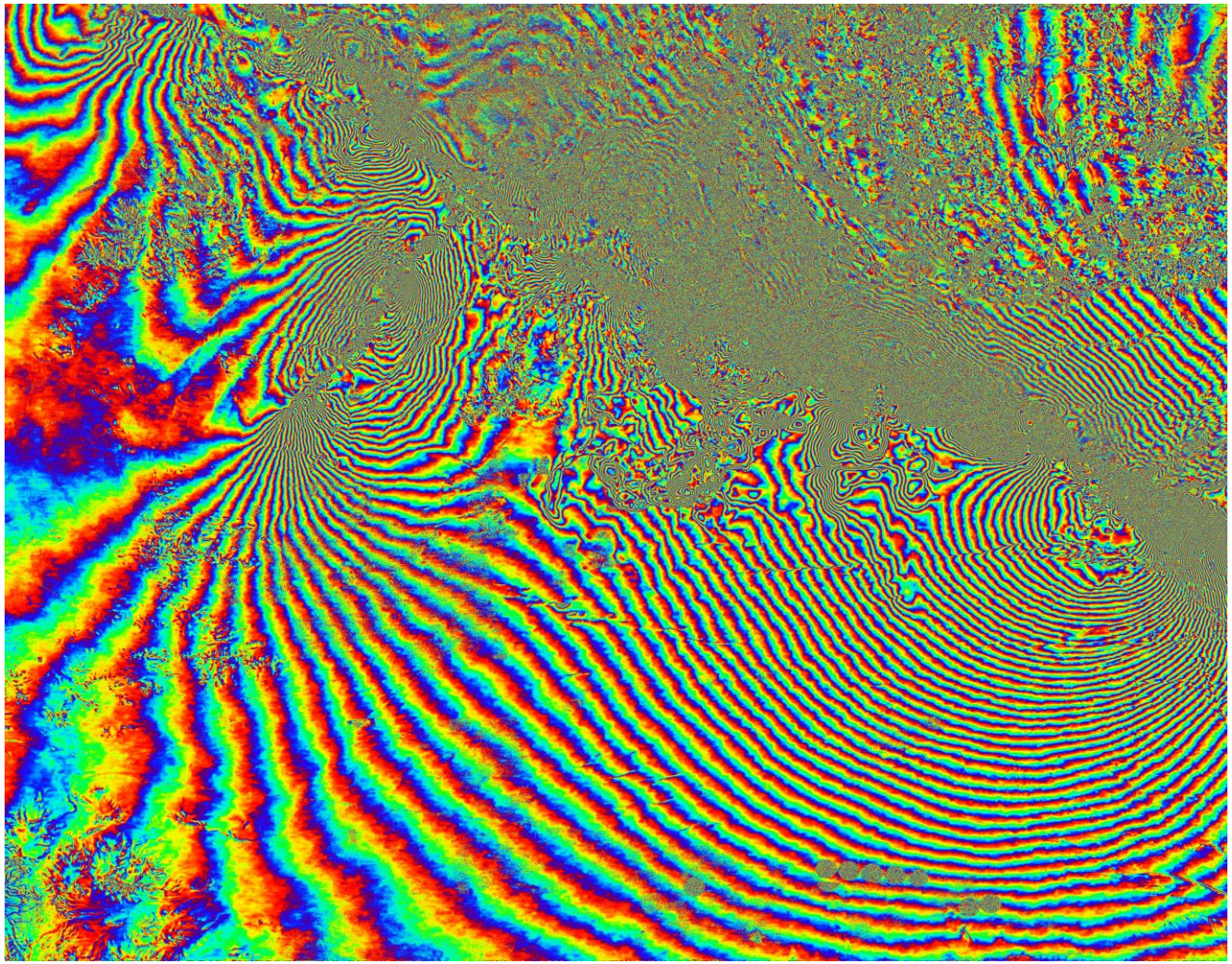

Temporal Decorrelation

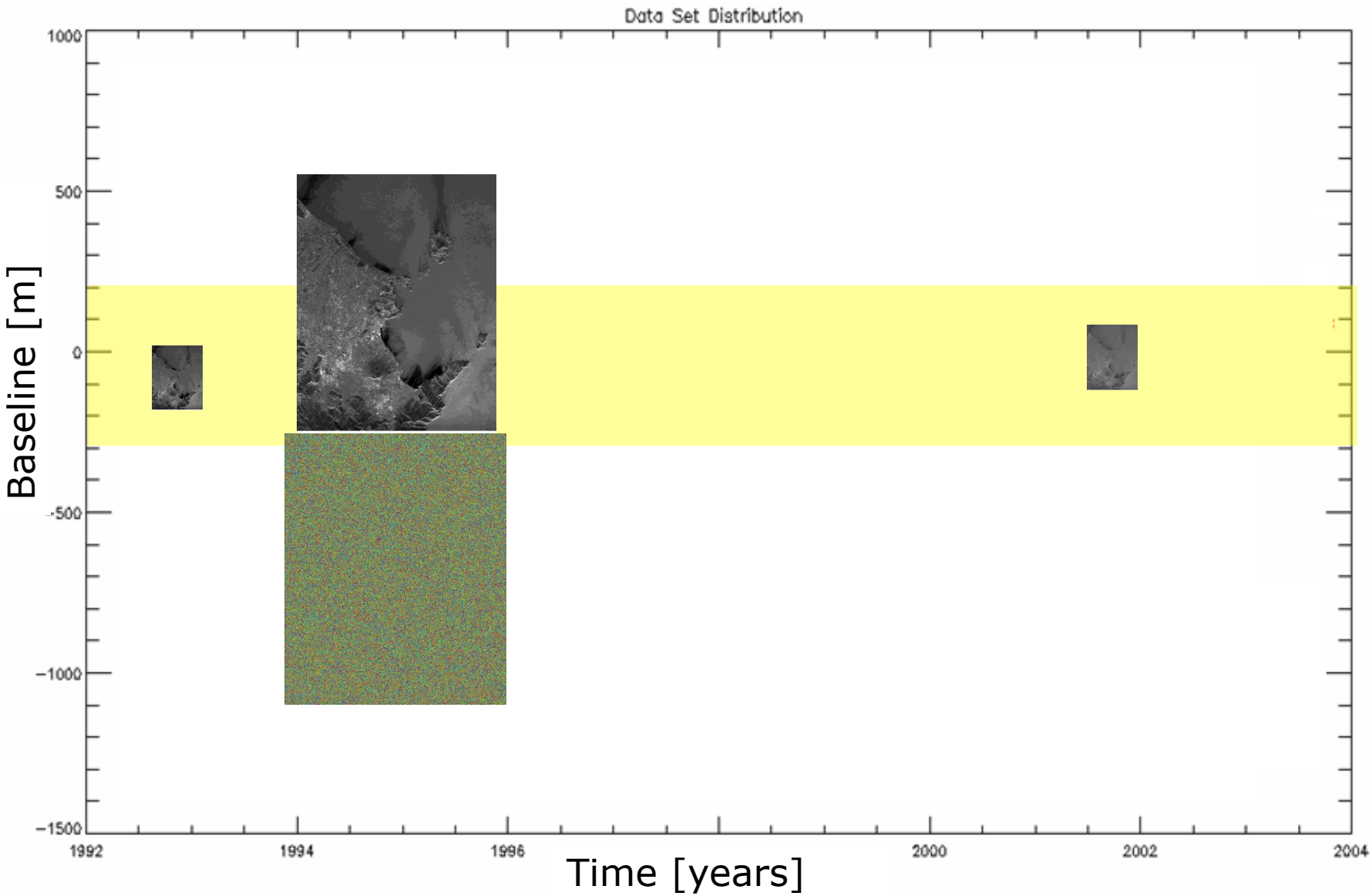

Spatial Decorrelation

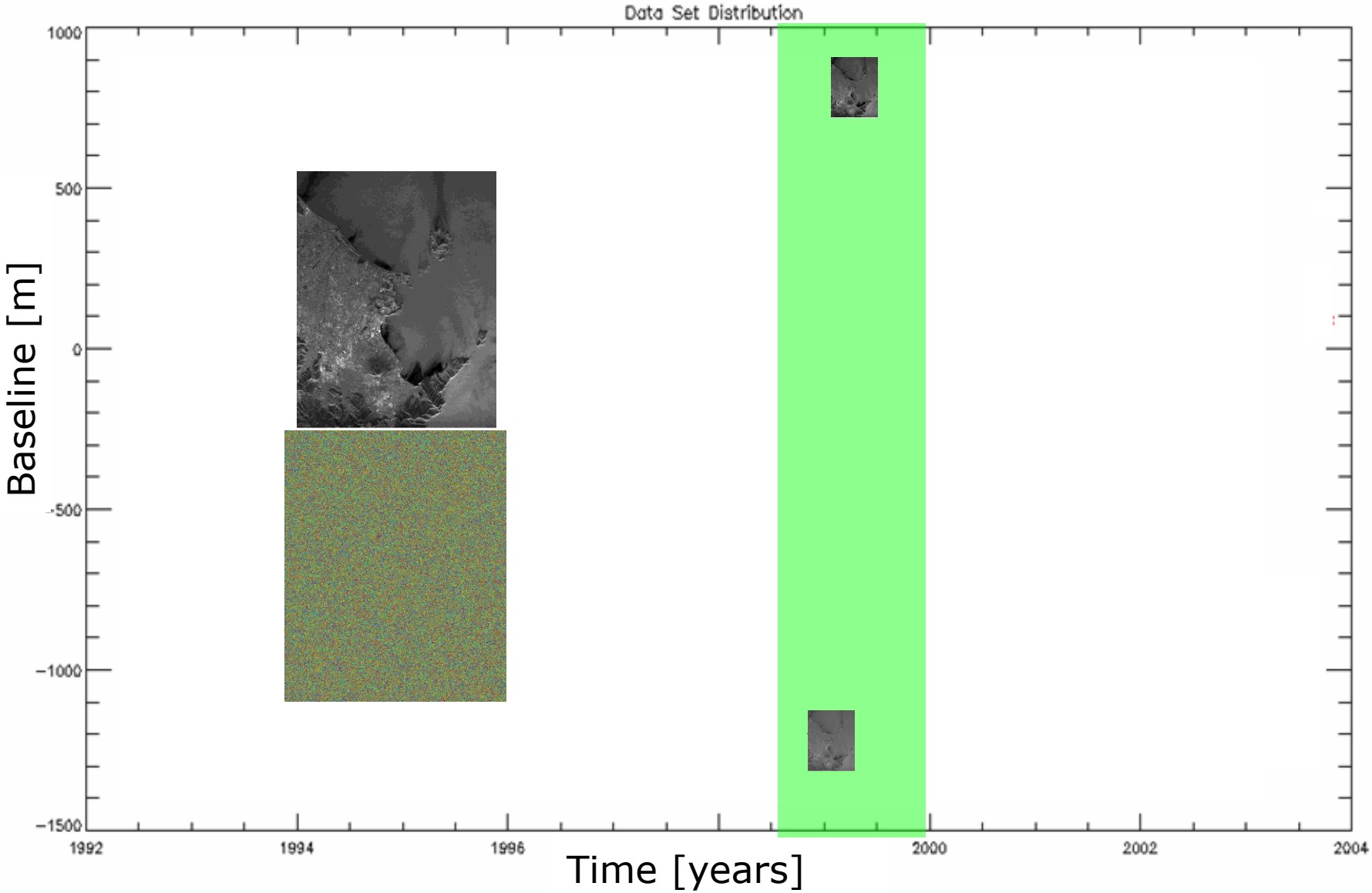

Small Baseline Interferogram

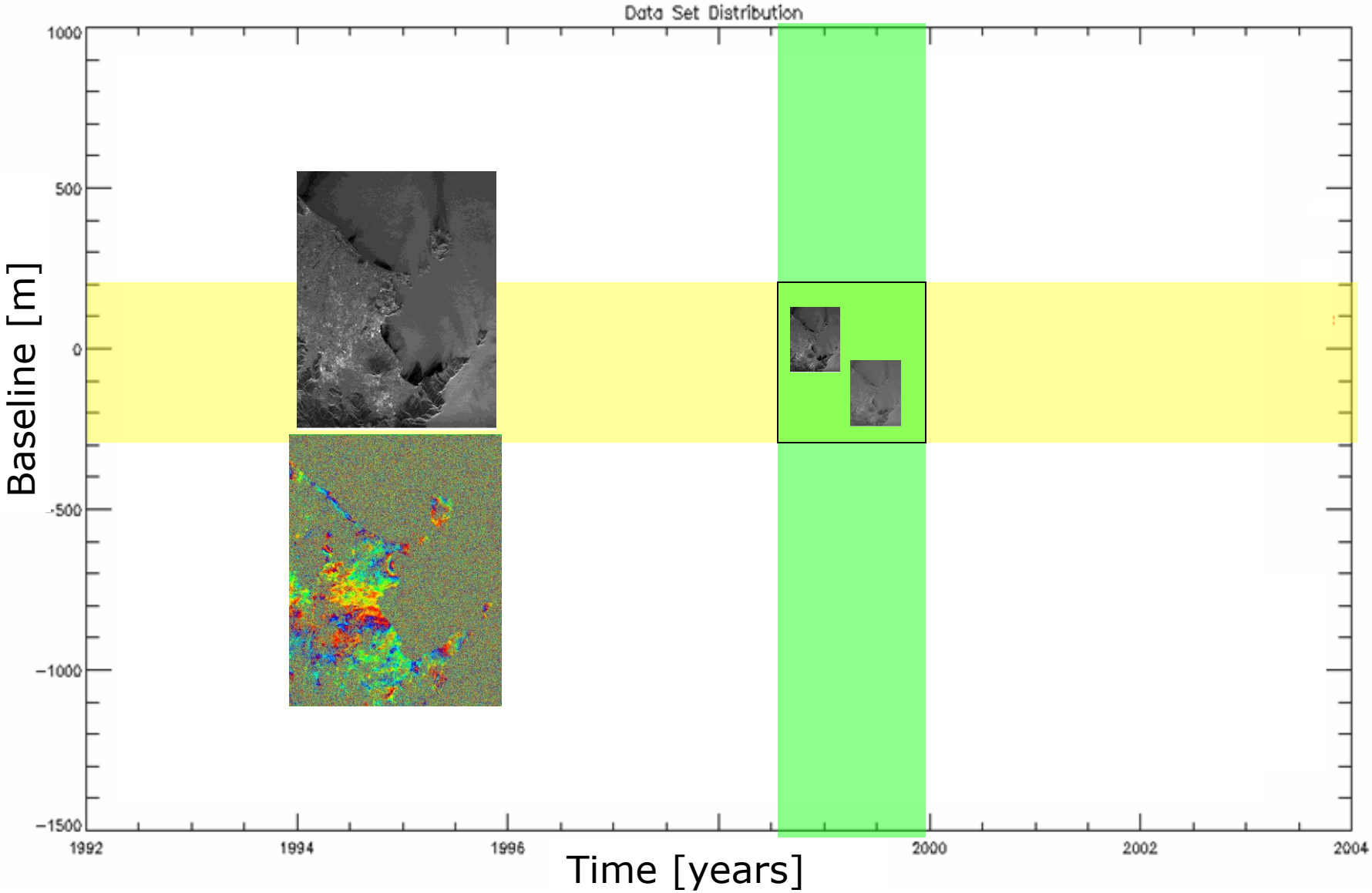

Main algorithms developed for time series generation

- Large Baseline
  - Permanent Scatterers (PS), POLIMI, Milan
  - Interferometric Point Target Analysis (IPTA), GAMMA, Switzerland
  - StamPS, Stanford University, Palo Alto
- Small Baseline
  - Small BAseline Subsets (SBAS), IREA-CNR, Naples
  - Choerent Pixels Technique (CPT), UPC, Barcelona
- Hybrids
  - SqueeSAR, TRE, Milan

Santa Ana: CSK Analysis

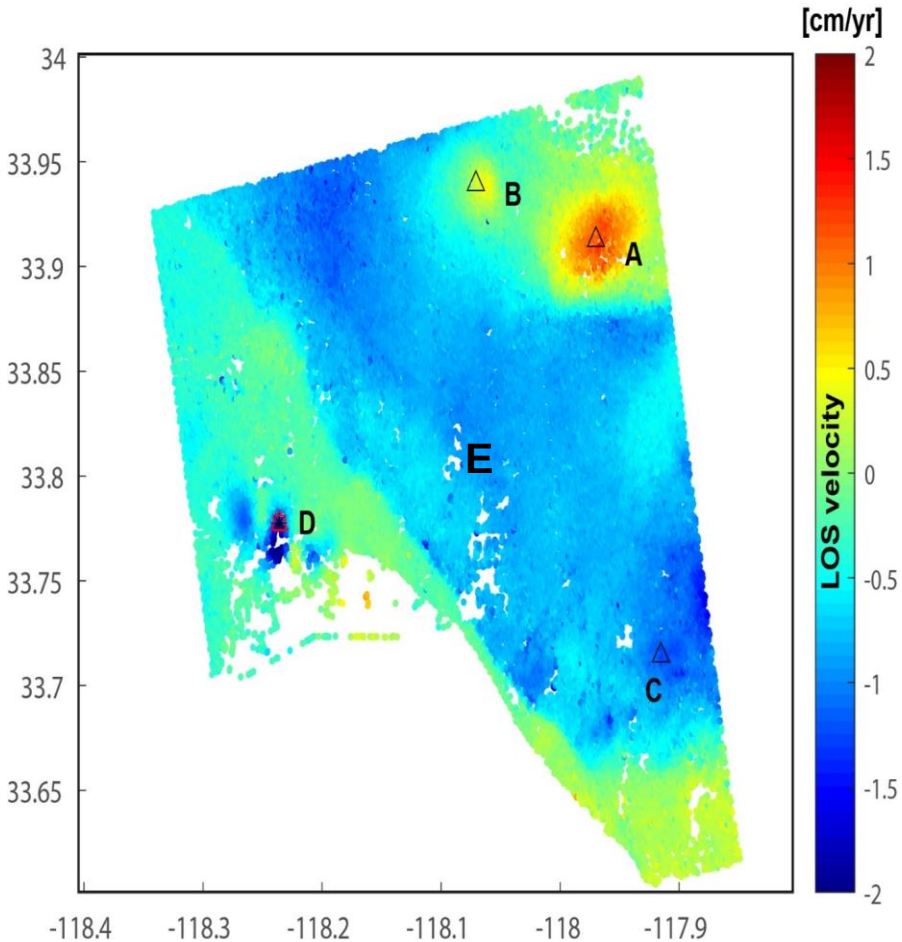

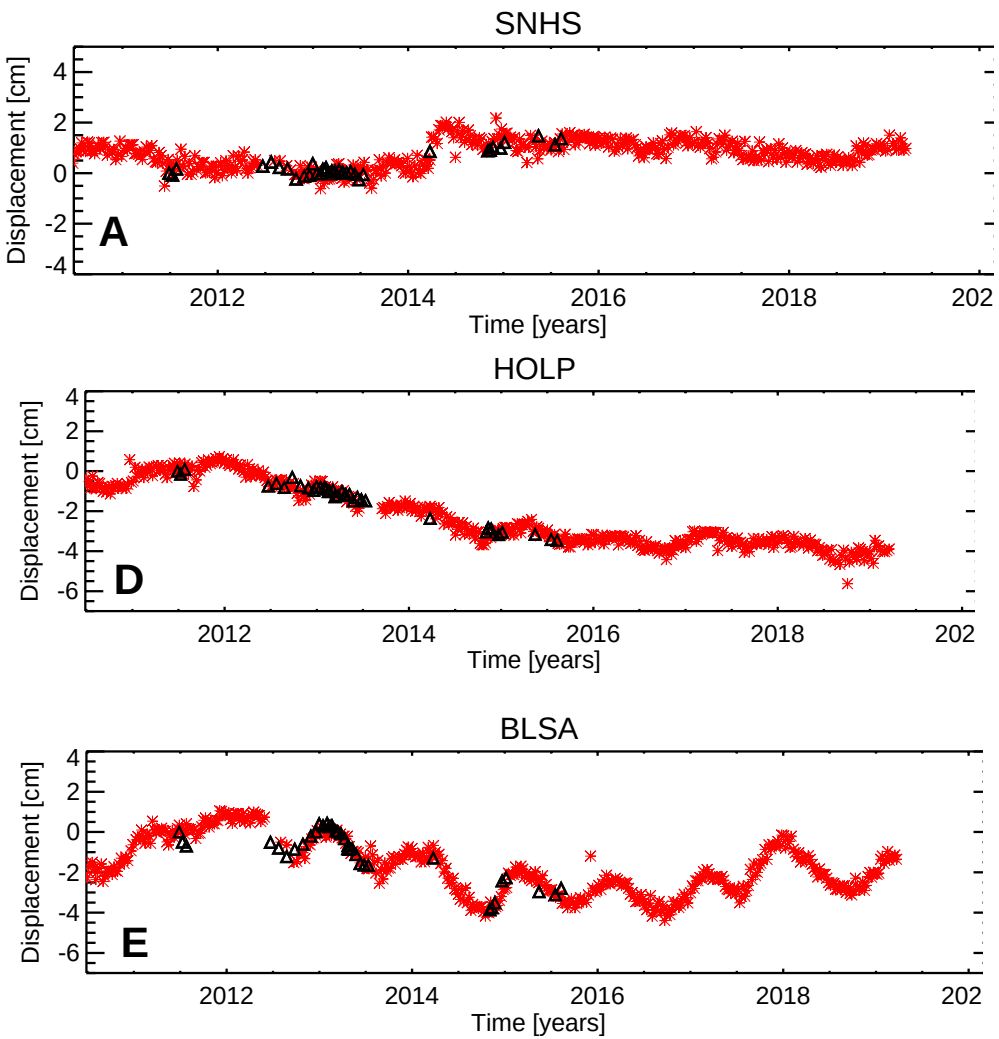

Burned Areas Mapping: Experiments with S-1

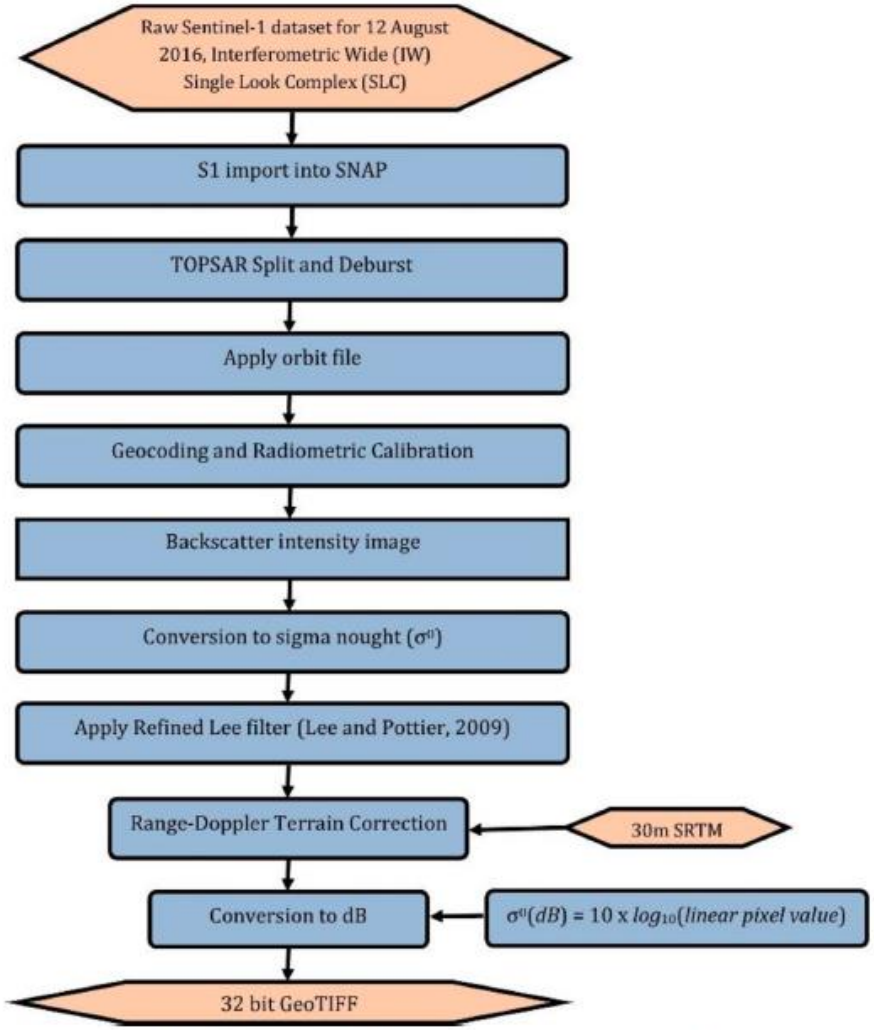

Fig. 2. Methodology work flow for the pre-processing of Sentinel 1.

Colson et al. 2018, "Exploring the Potential of Sentinels-1 & 2 of the Copernicus Mission in Support of Rapid and Cost-effective Wildfire Assessment," Int J Appl Earth Obs Geoinformation 73 (2018) 262–276

Map of burned areas (Mt. Vesuvius)

Map of burned areas (Mt. Vesuvius)

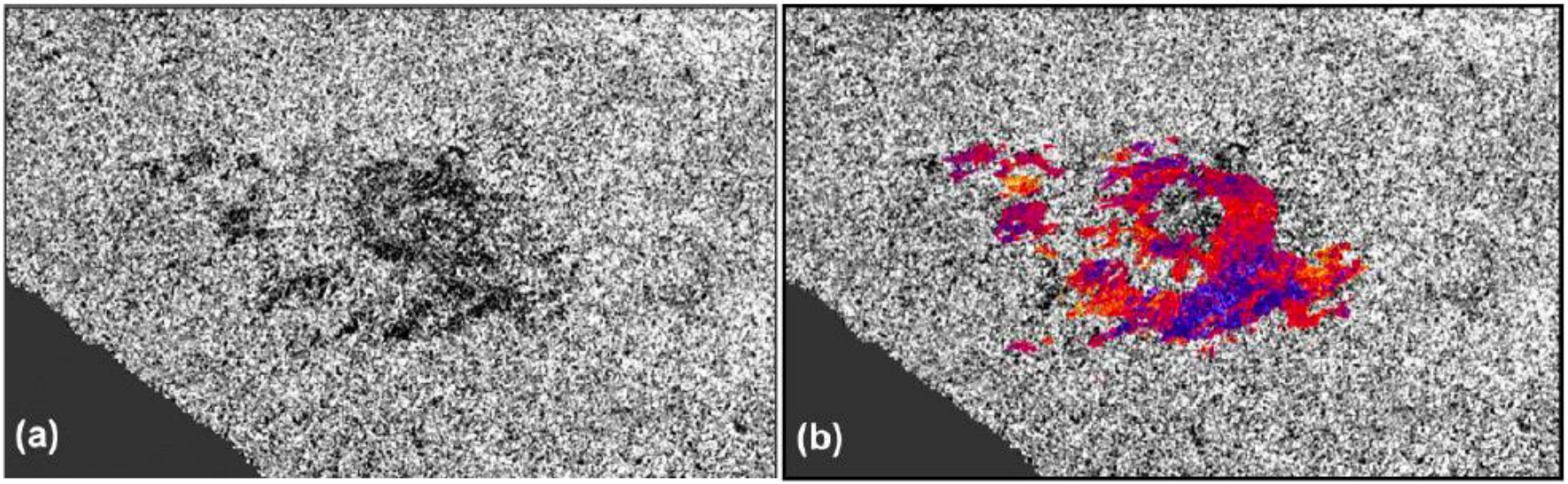

Figura 3. (a) Log-Ratio map of the May-September S-1 radiometrically calibrated SAR images. (b) Comparison between the map and the burned areas as derived from the Copenicus Emergency Management system catalogue.

June 12, 2017 – September 16, 2017 Sigma Nought Difference

Coherent Change Detection Analysis

Detection of changes caused by major events, such as earhquakes, volcanic eruptions and floods from SAR/InSAR data is challenging because the temporal decorrelation caused by natural phenomena

$$\gamma = \frac{\langle s_1 \, s_2^* \rangle}{\sqrt{\langle s_1 \, s_1^* \rangle \, \langle s_2 \, s_2^* \rangle}}$$

$$\gamma = \gamma_{\text{geometric}} \gamma_{\text{thermal}} \gamma_{\text{temporal\&volume}} \cdot$$

$$\gamma_{\text{thermal}} = \frac{1}{1 + \text{SNR}^{-1}} \cdot$$

Coherent Change Detection Analysis

Volumetric decorrelation originates from the scattering of radar microwaves within a volume, such as forest canopies. Recent research efforts using polarimetric SAR interferometry aim at retrieving the structural parameters of forests using a two-layer model in which the properties of coherence and interferometric phase are sensitive to forest vertical structure and height.

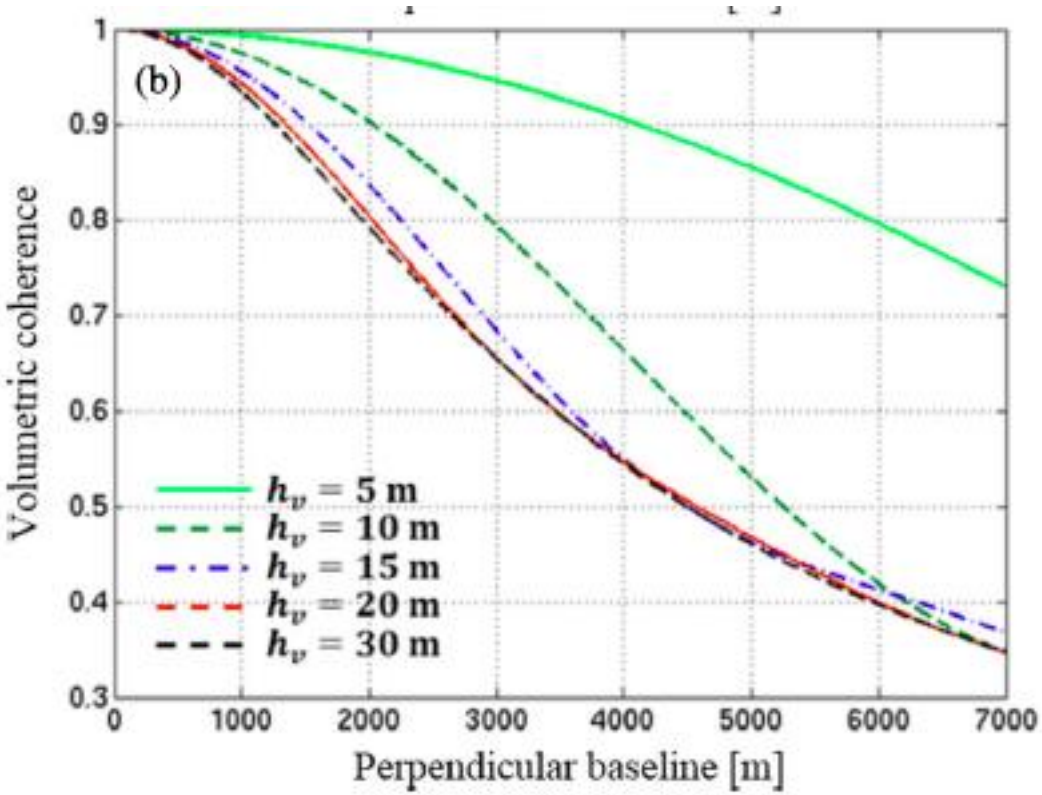

Random-volume-over-ground (RVoG) model

Temporal Decorrelation Model

$$\gamma_{d,\mathrm{time}} = \exp\left(-\frac{\Delta T}{\tau}\right)$$

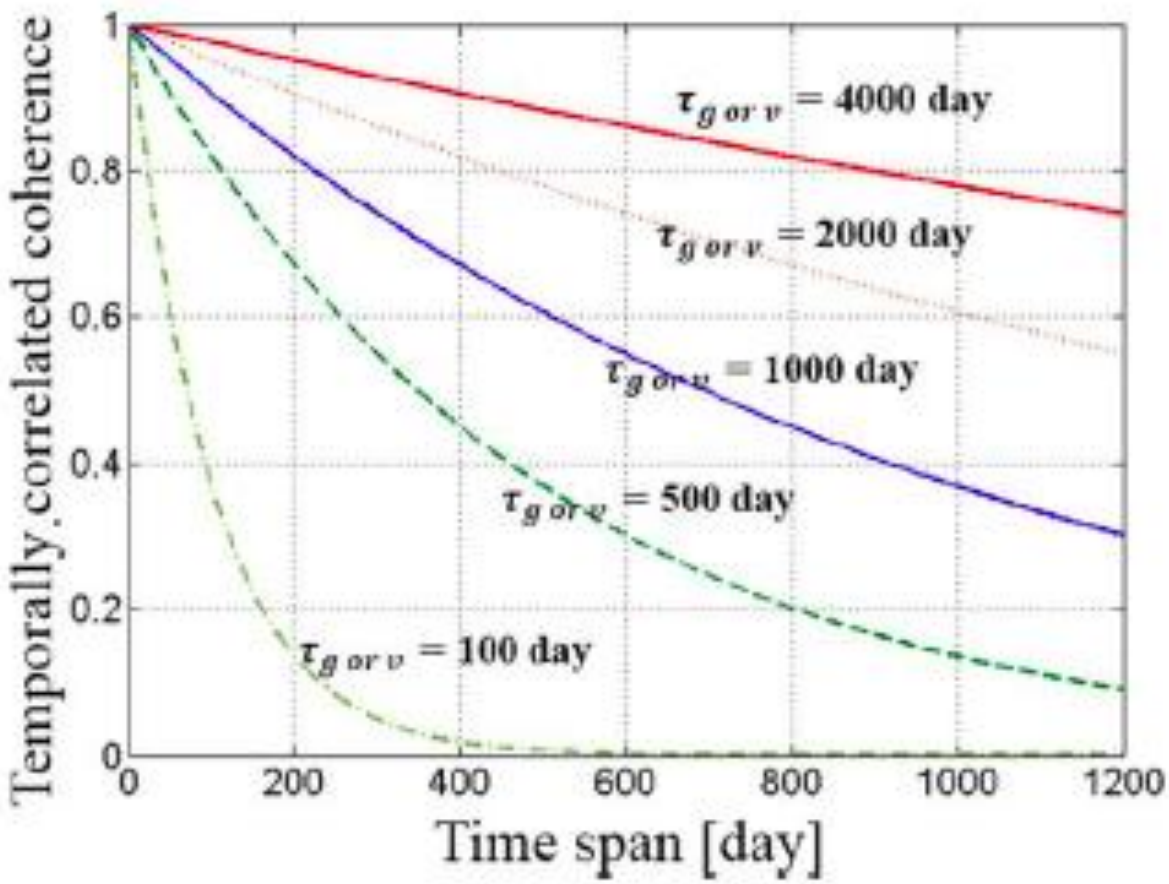

Coherent Change Detection Analysis

One of the most powerful techniques for disaster response using SAR imagery is coherent change detection (CCD). This technique is based on the interferometric coherence (correlation) between two complex images acquired before and after a disaster event. The interferometric coherence has been known as a detector very sensitive to subtle changes induced by dielectric properties and disturbance of scatterers in a resolution cell.

Burned Areas Detection

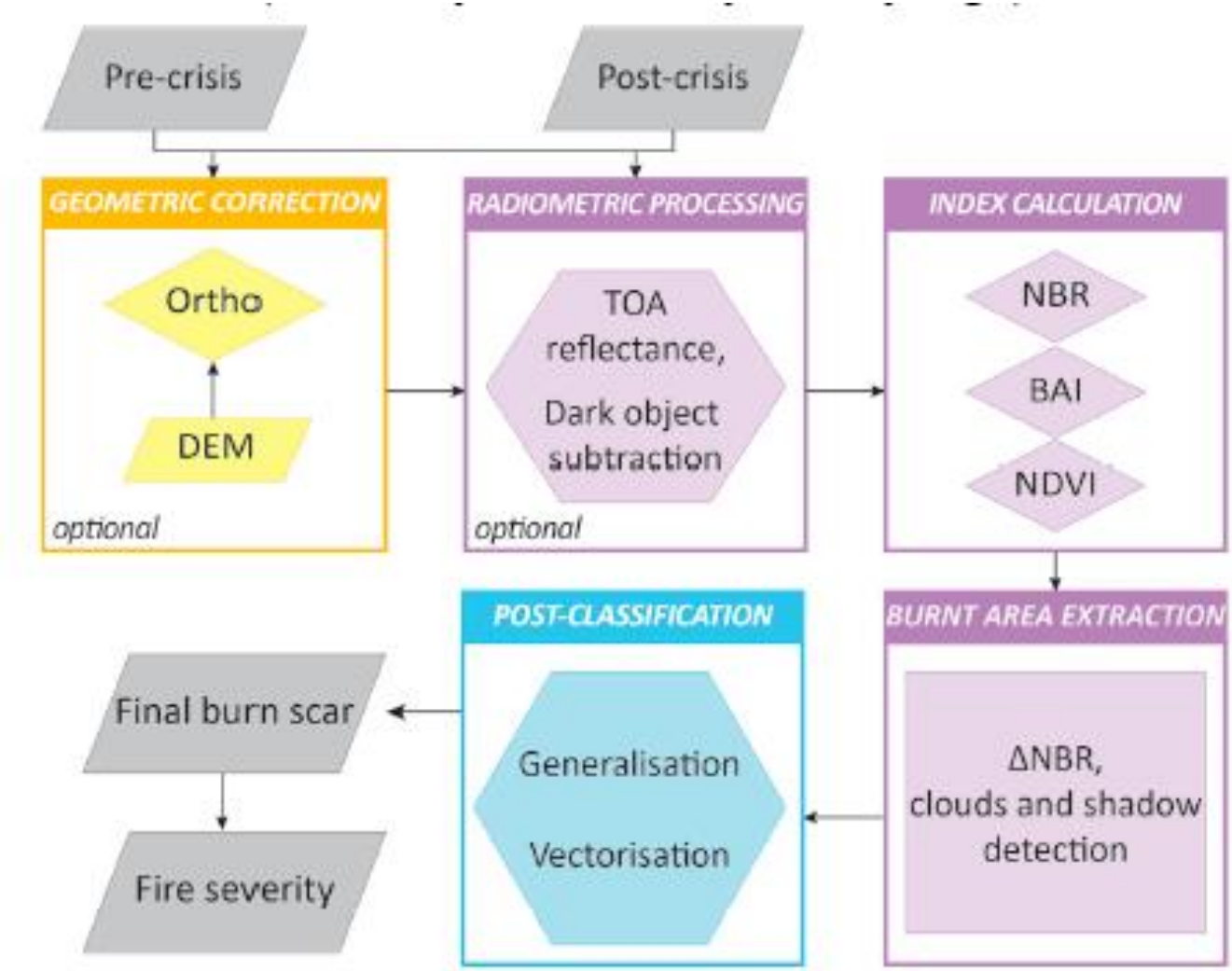

Fig. 1: BURNOUT workflow.

Burned Areas Detection

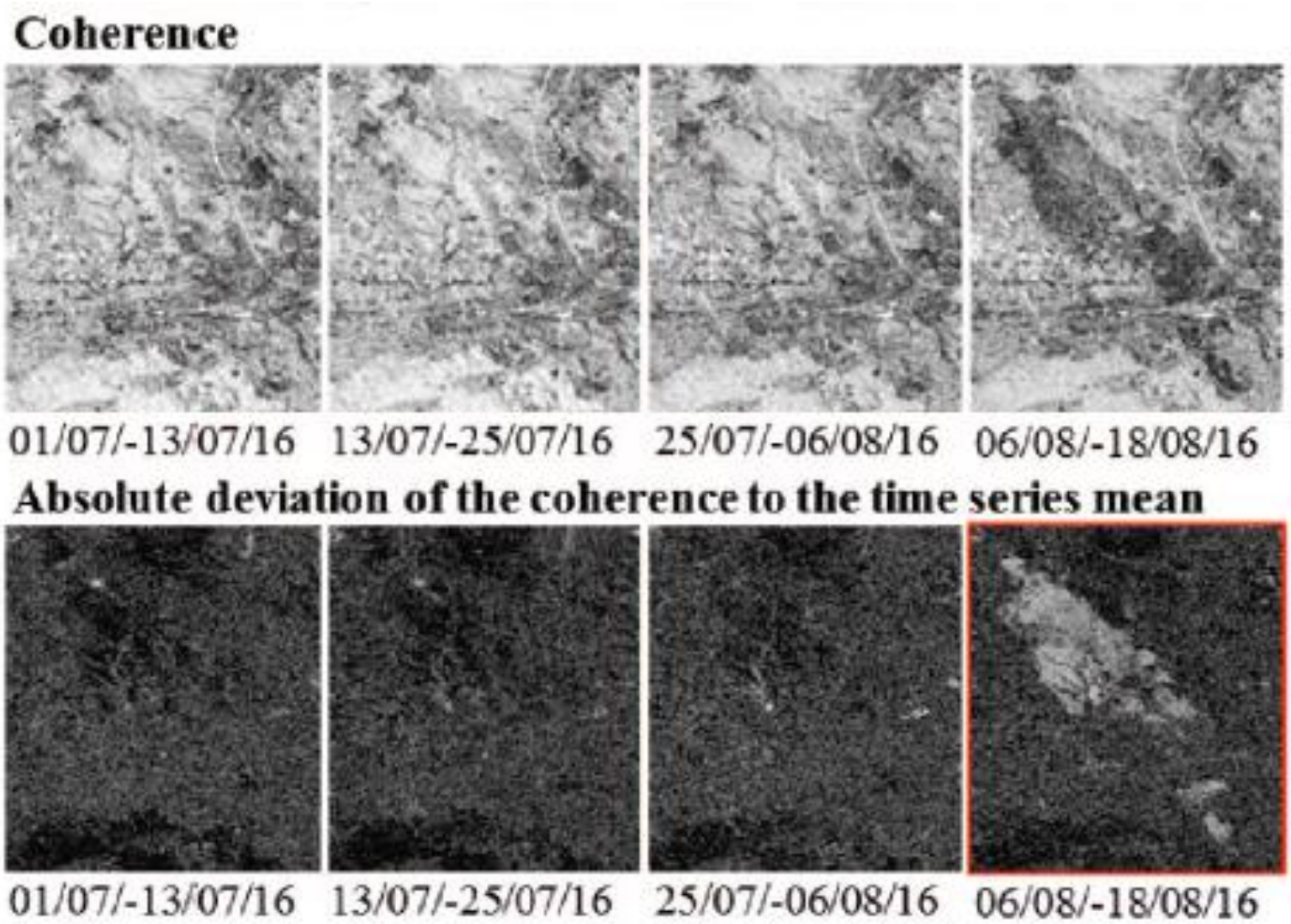

… the problem is hard

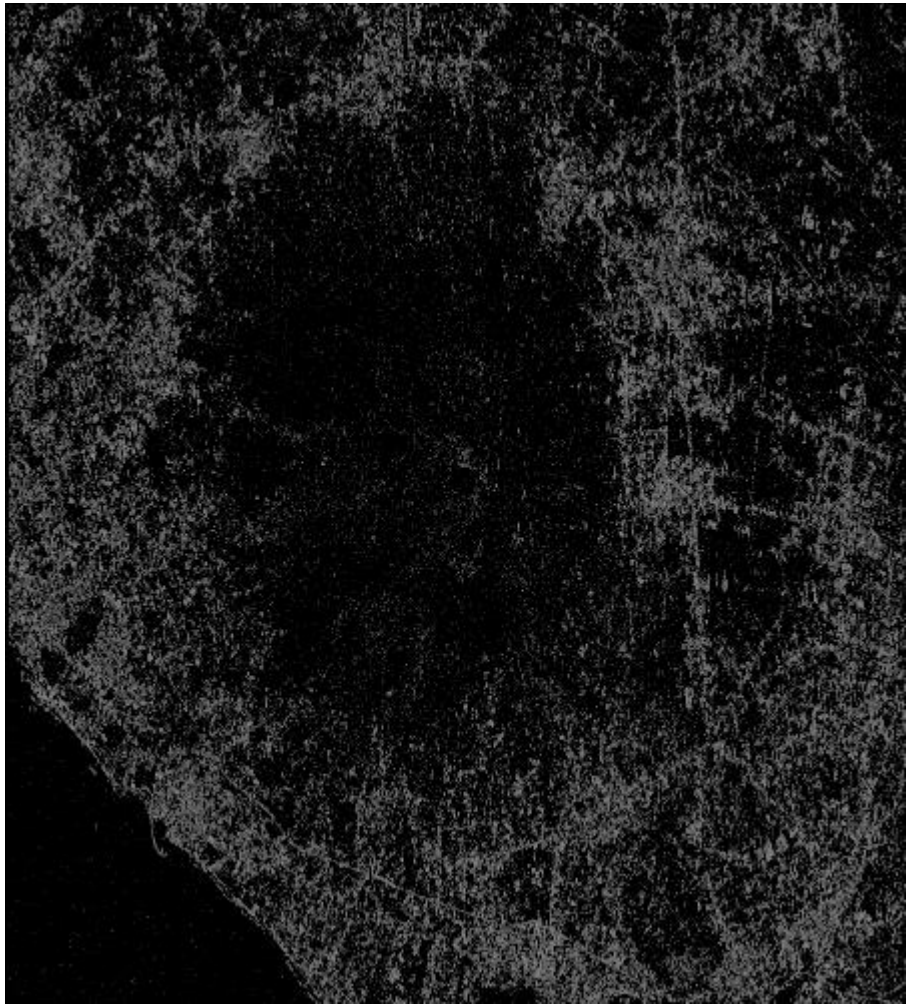

18/04/2017_25/04/2017

Burned Areas: Mt Vesuvius

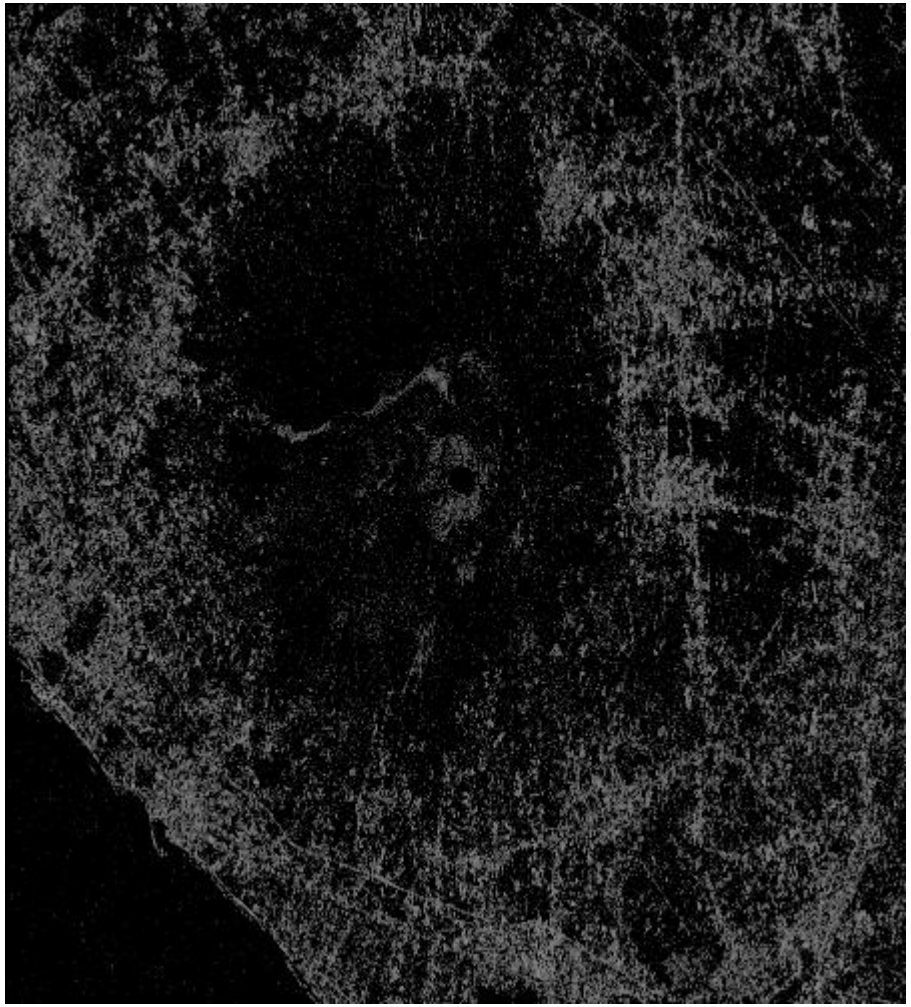

25/04/2017_30/04/2017

Burned Areas: Mt Vesuvius

30/04/2017_06/05/2017

Burned Areas: Mt Vesuvius

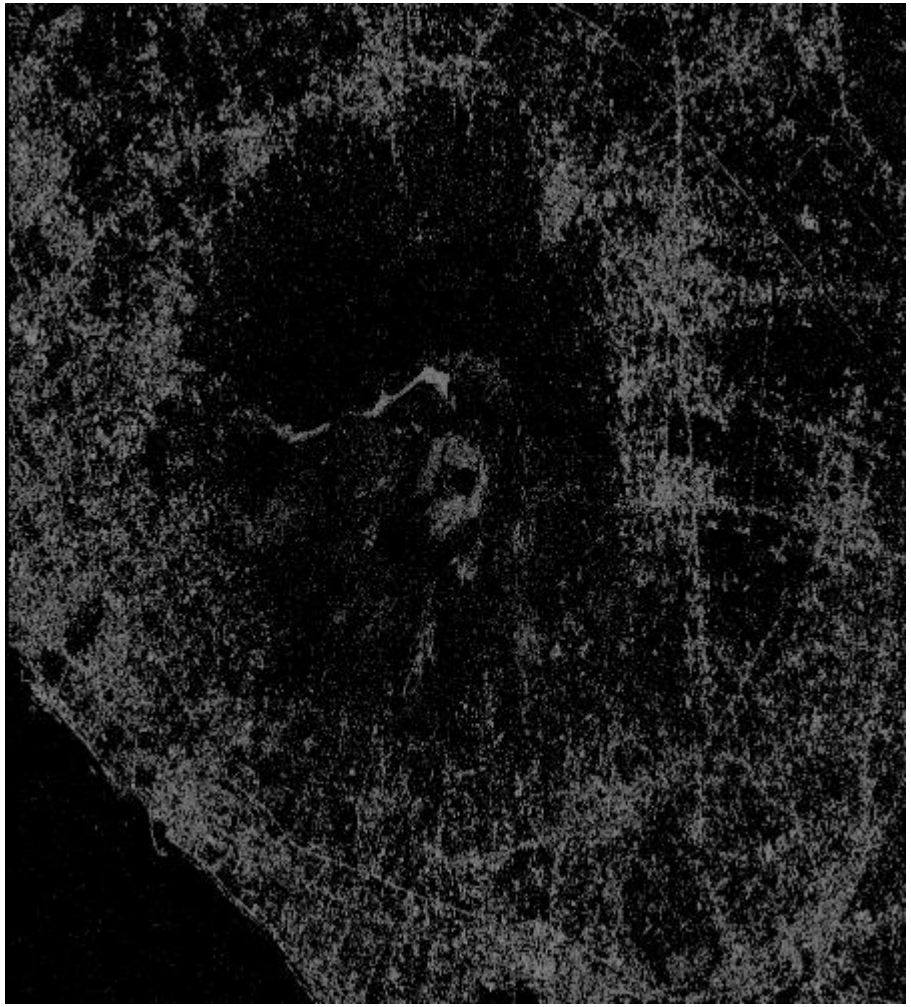

06/05/2017_12/05/2017

Burned Areas: Mt Vesuvius

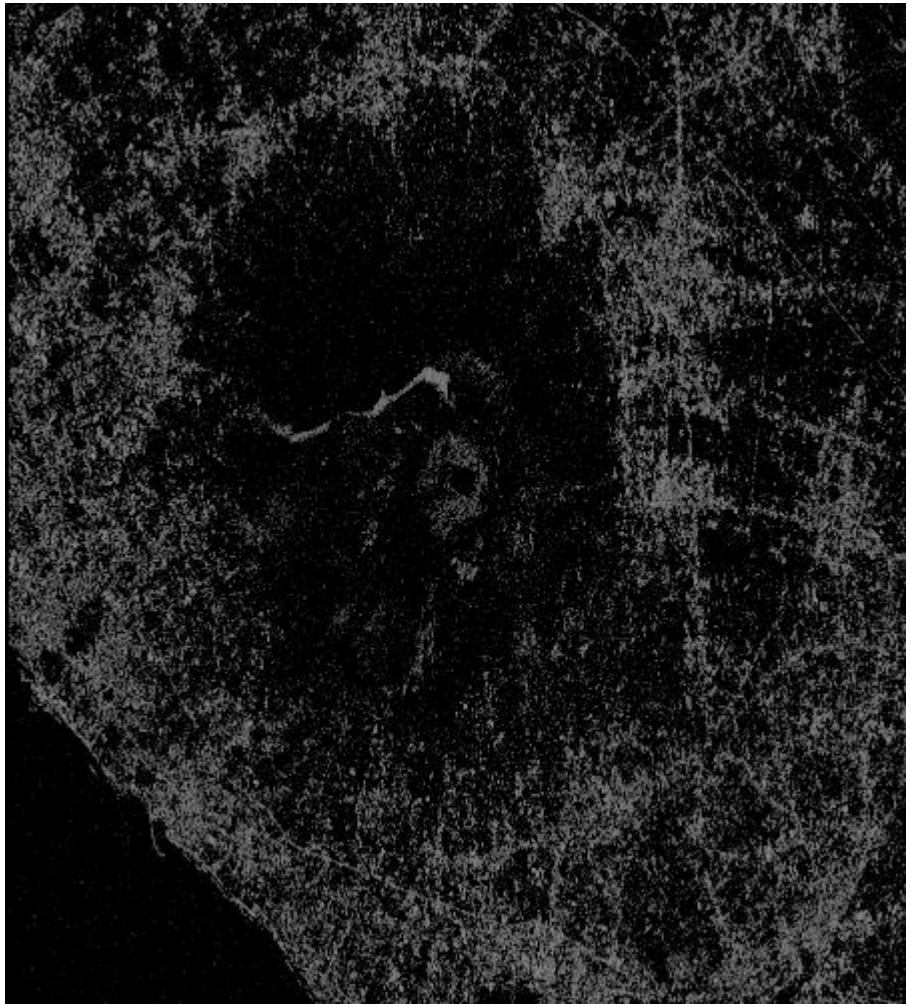

12/05/2017_18/05/2017

Burned Areas: Mt Vesuvius

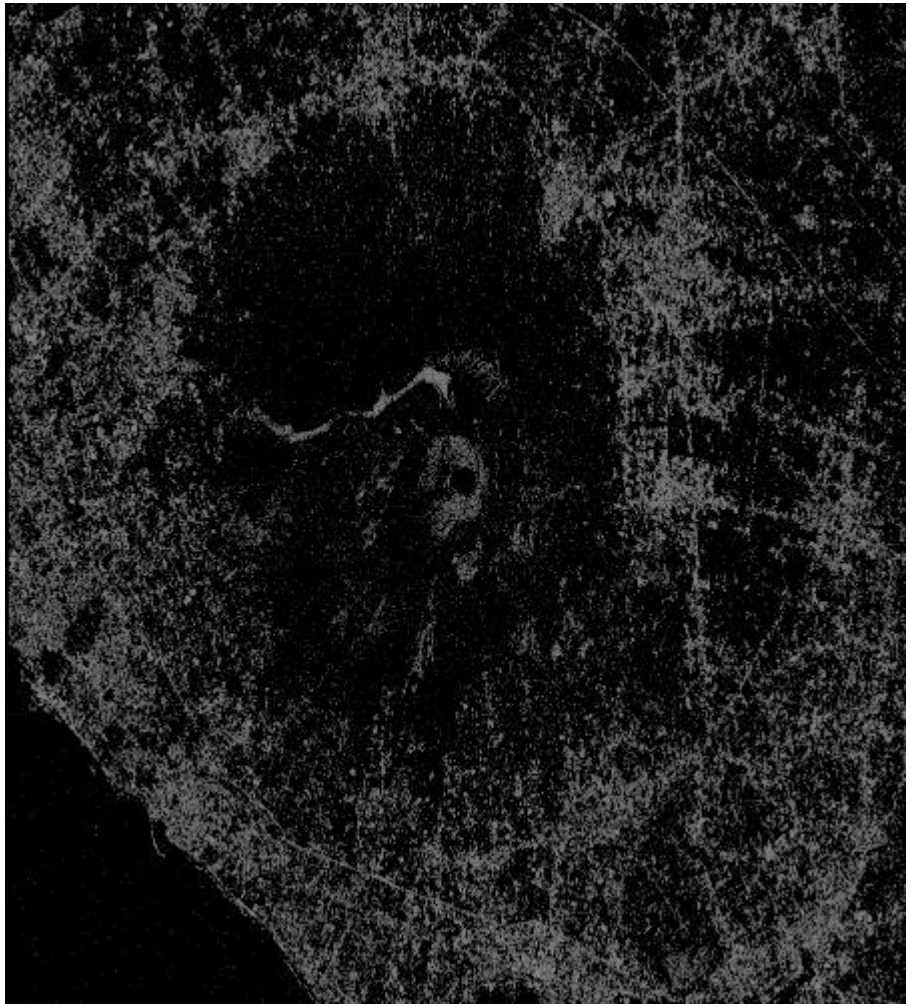

18/05/2017_24/05/2017

Burned Areas: Mt Vesuvius

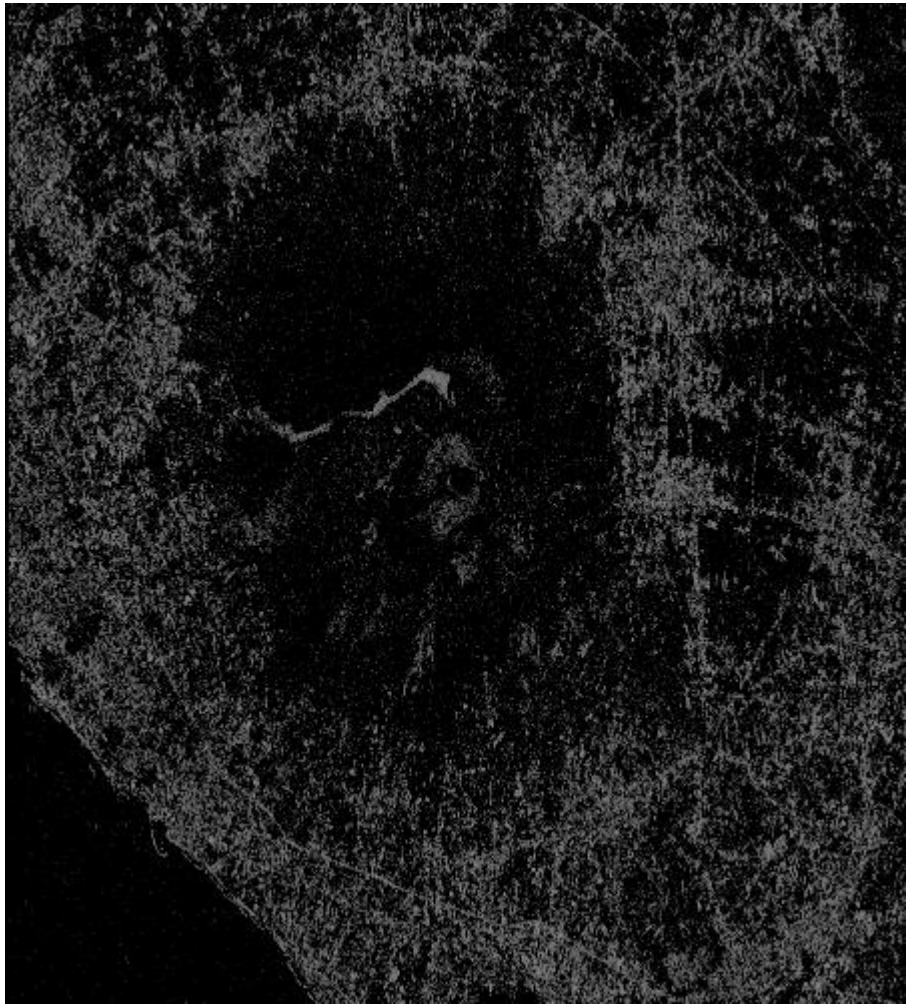

24/05/2017_30/05/2017

Burned Areas: Mt Vesuvius

30/05/2017_05/06/2017

Burned Areas: Mt Vesuvius

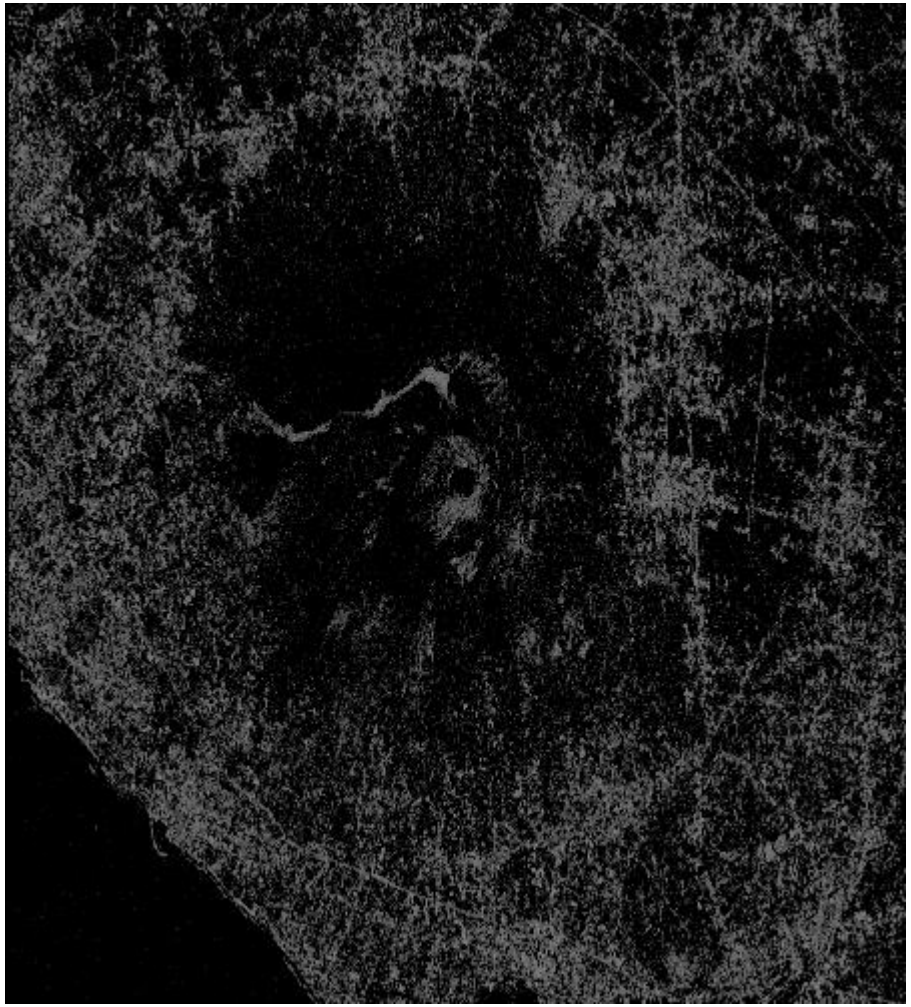

05/06/2017_11/06/2017

Burned Areas: Mt Vesuvius

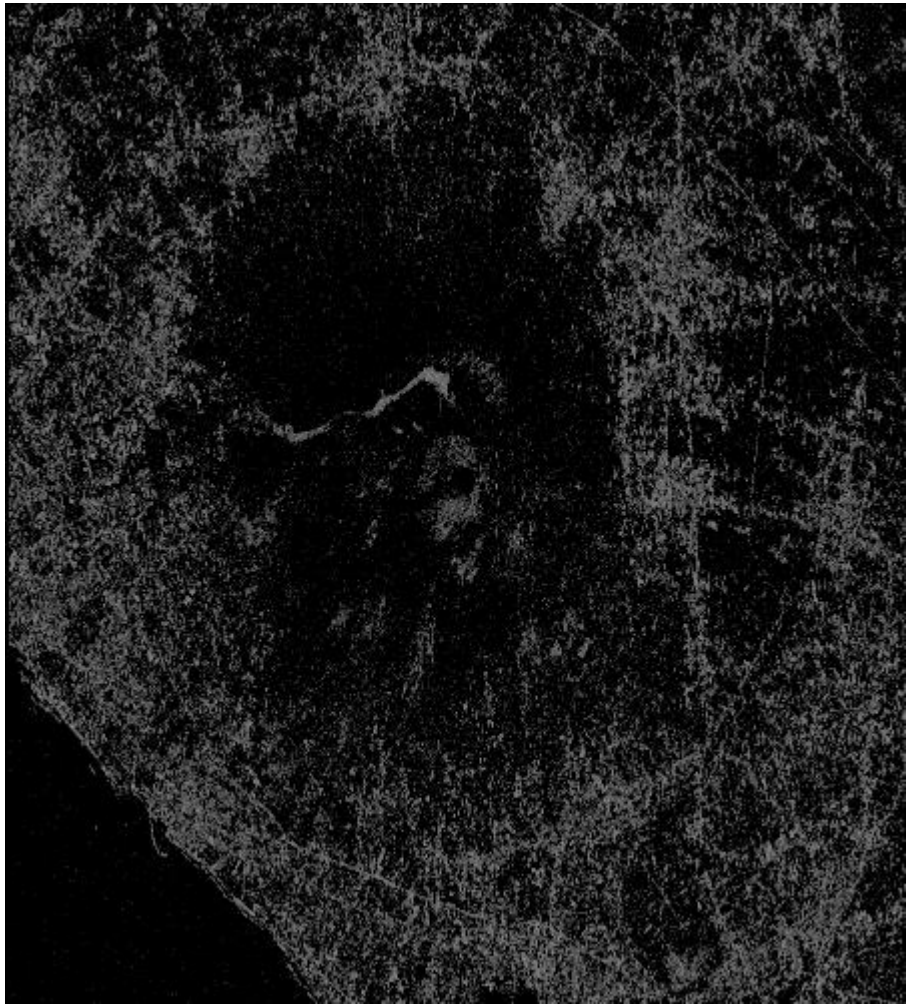

11/06/2017_17/06/2017

Burned Areas: Mt Vesuvius

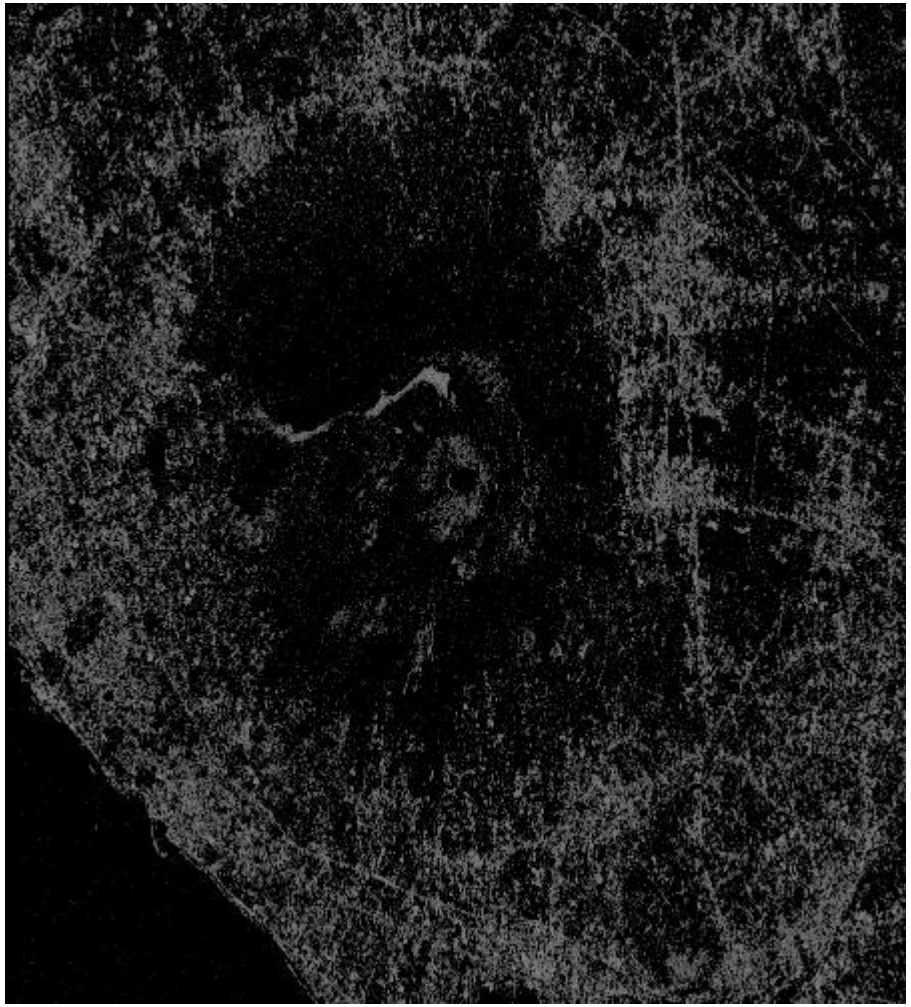

17/06/2017_23/06/2017

Burned Areas: Mt Vesuvius

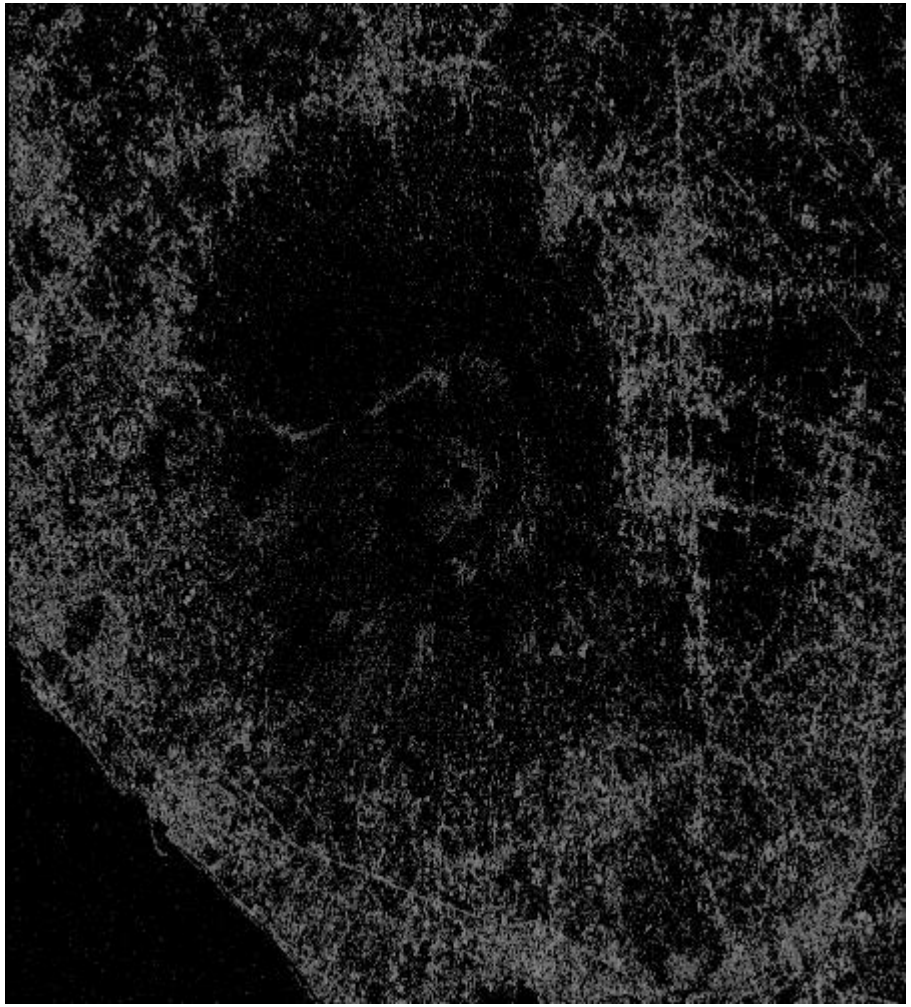

23/06/2017_29/06/2017

Burned Areas: Mt Vesuvius

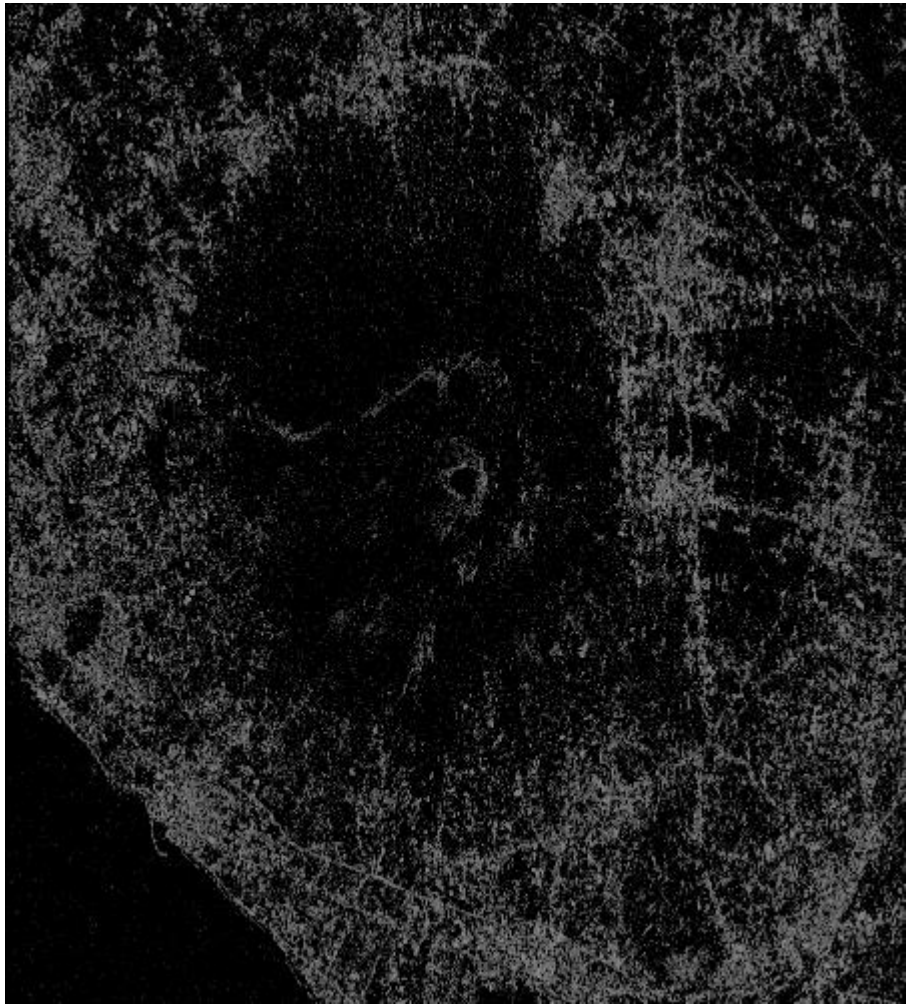

29/06/2017_05/07/2017

Burned Areas: Mt Vesuvius

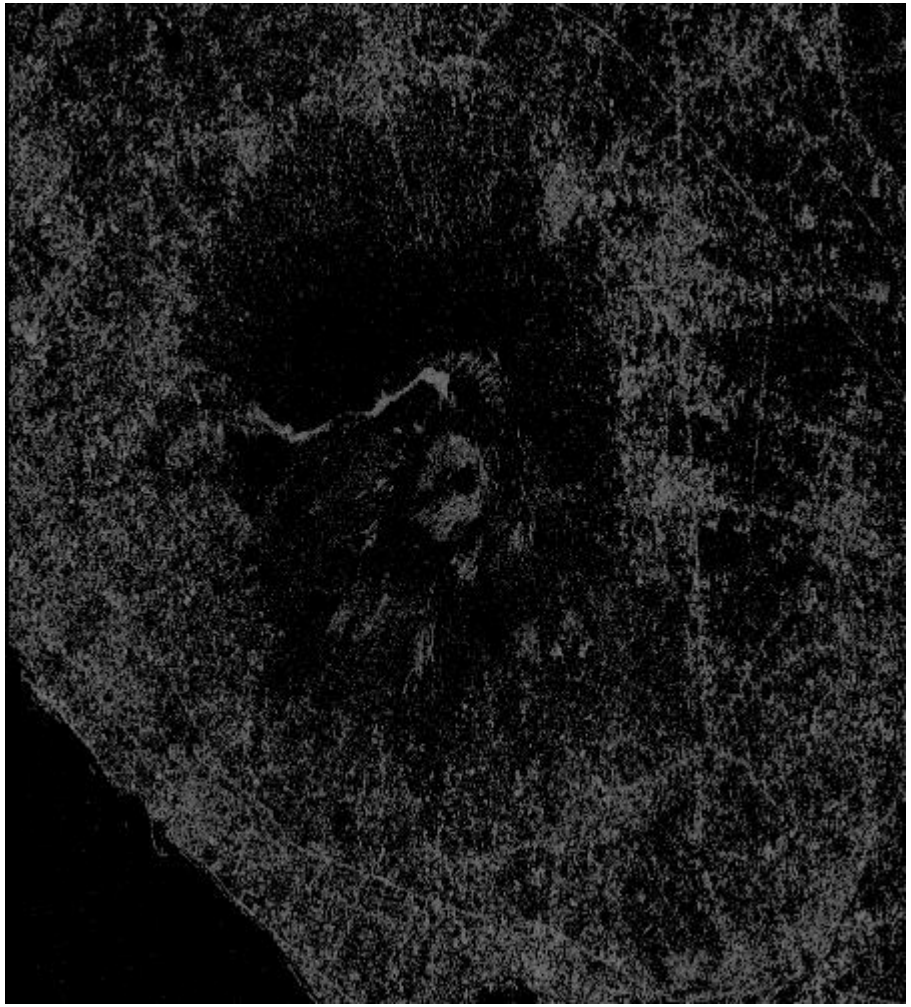

05/07/2017_11/07/2017

Burned Areas: Mt Vesuvius

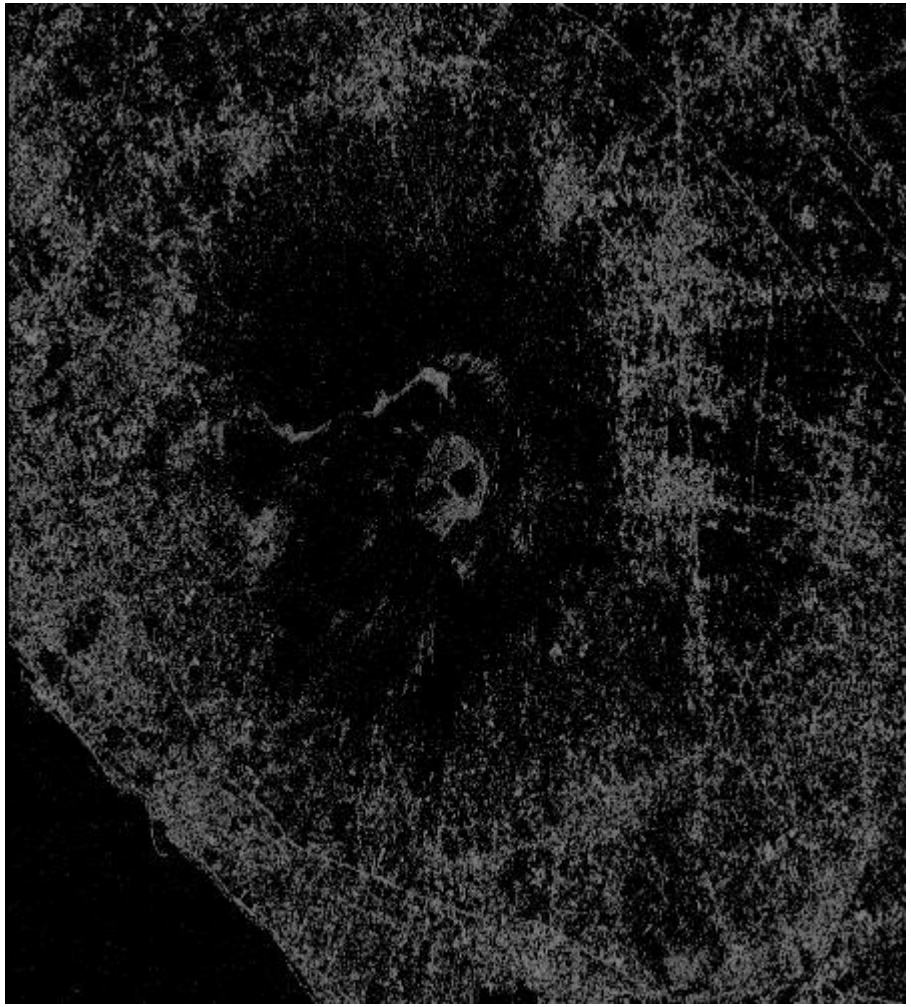

11/07/2017_17/07/2017

Burned Areas: Mt Vesuvius

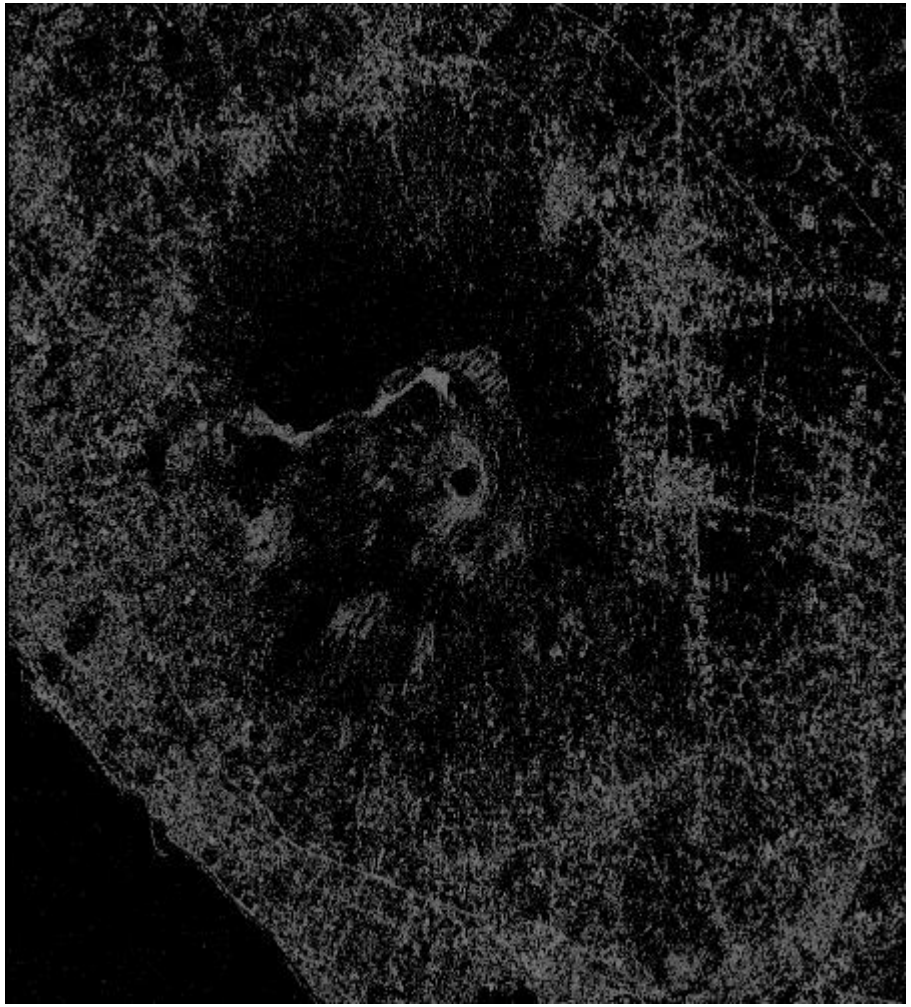

17/07/2017_23/07/2017

Burned Areas: Mt Vesuvius

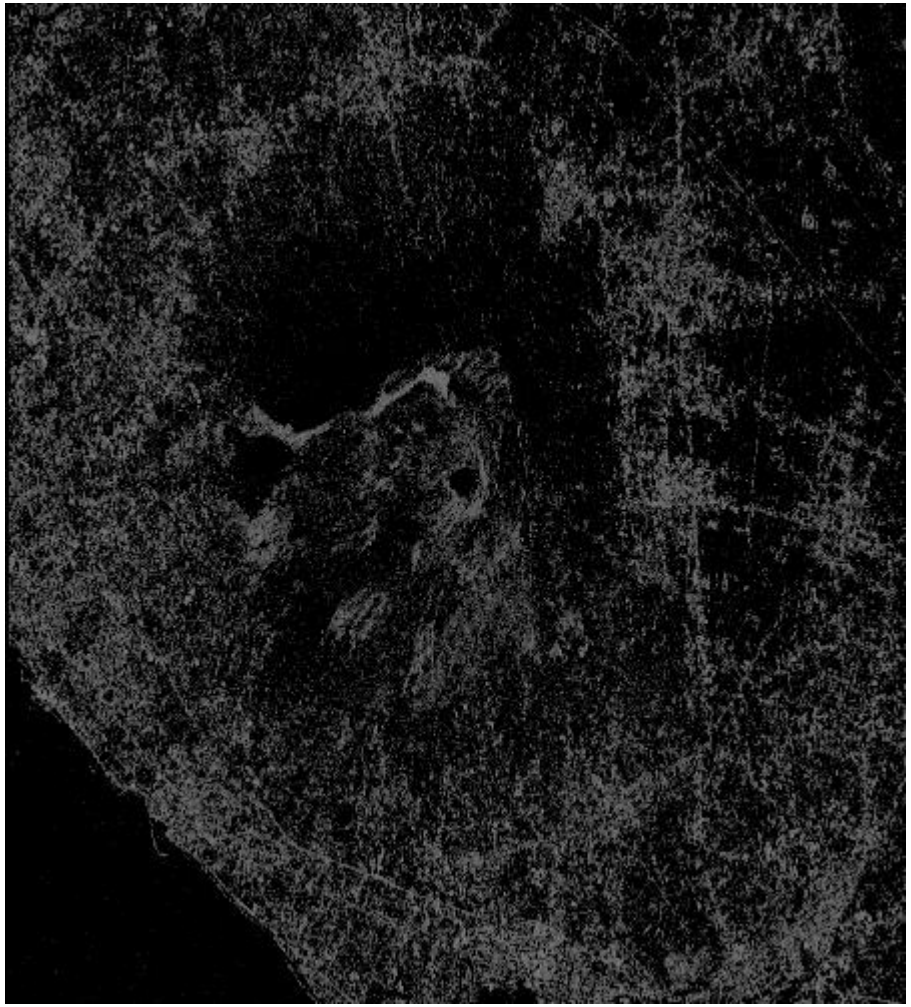

23/07/2017_29/07/2017

Burned Areas: Mt Vesuvius

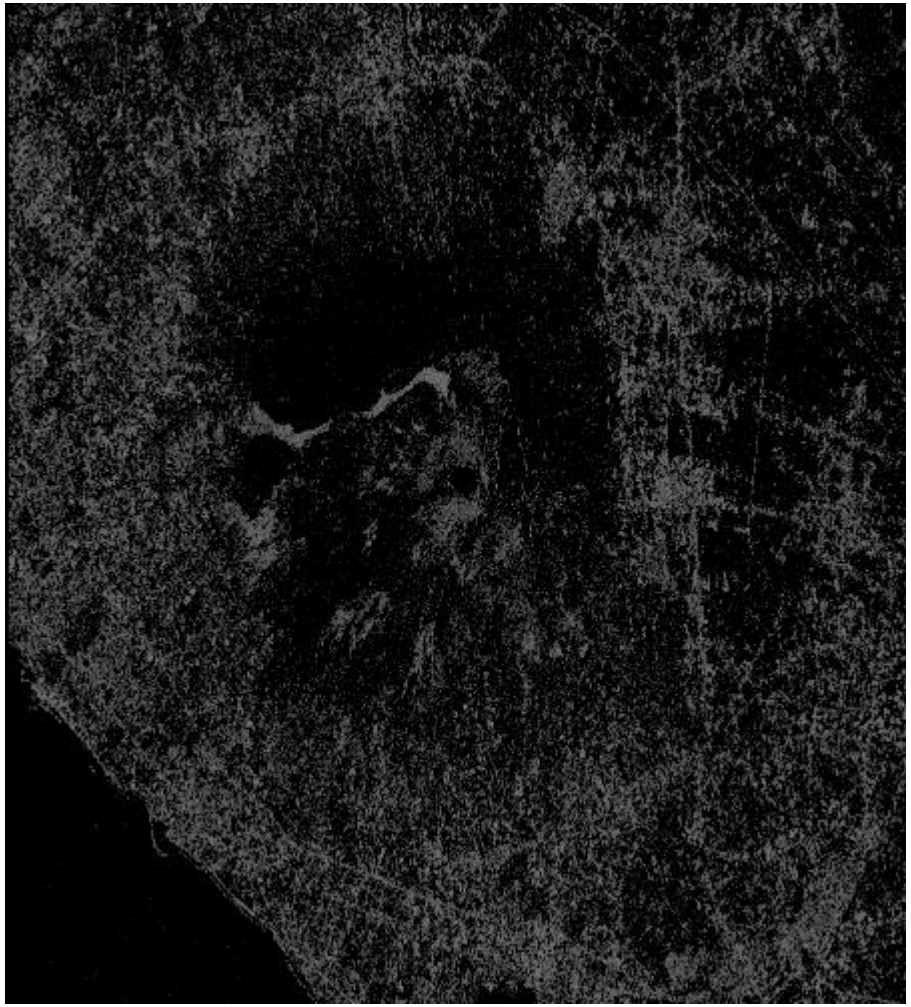

29/07/2017_04/08/2017

Burned Areas: Mt Vesuvius

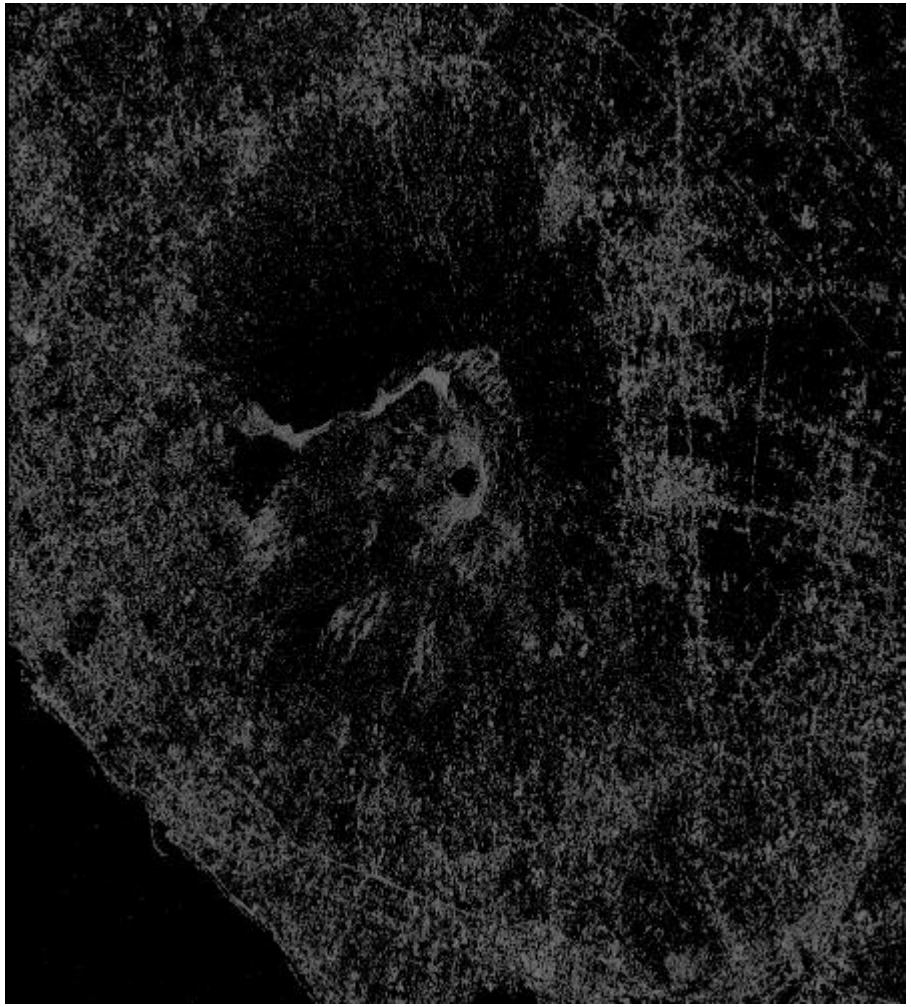

04/08/2017_10/08/2017

Burned Areas: Mt Vesuvius

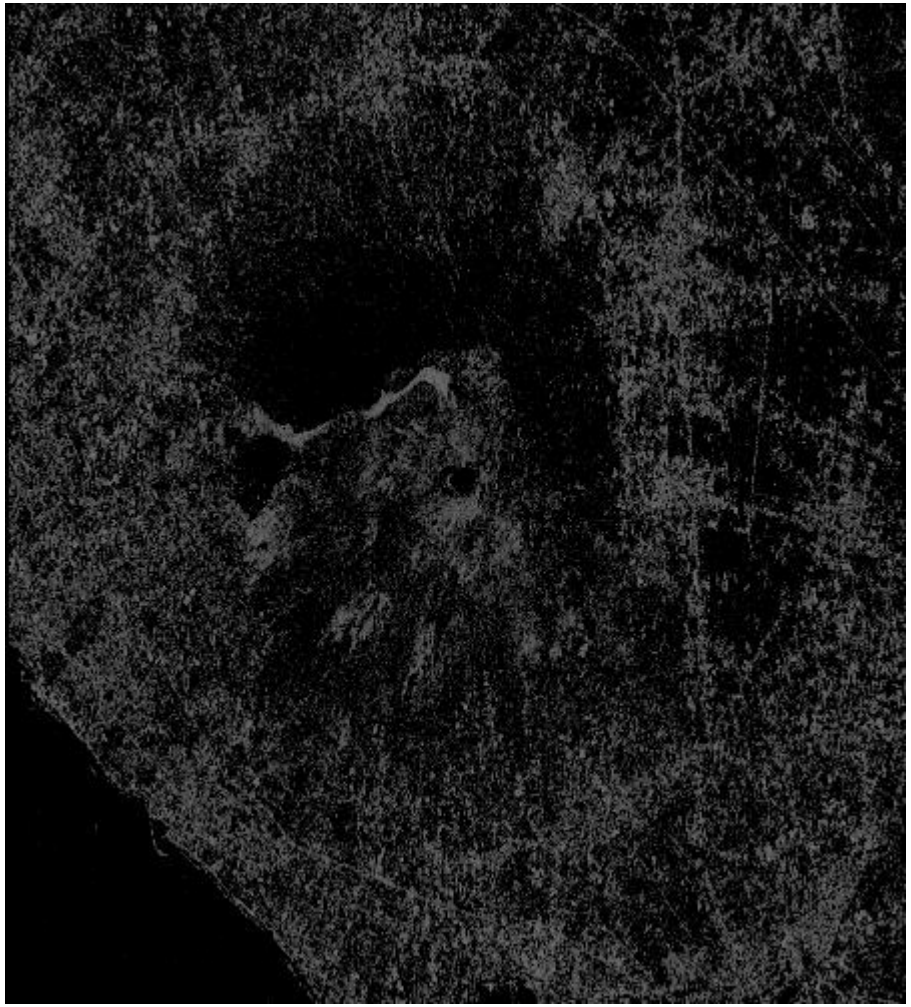

10/08/2017_16/08/2017

Burned Areas: Mt Vesuvius

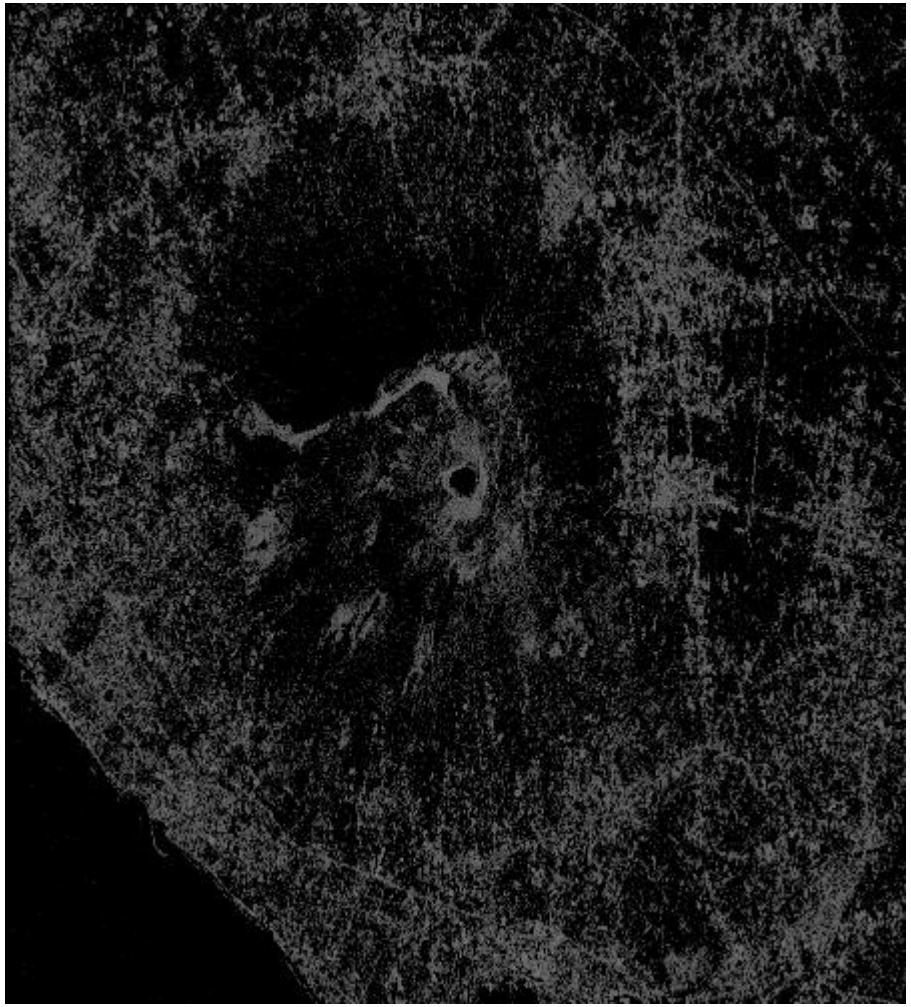

16/08/2017_22/08/2017

Burned Areas: Mt Vesuvius

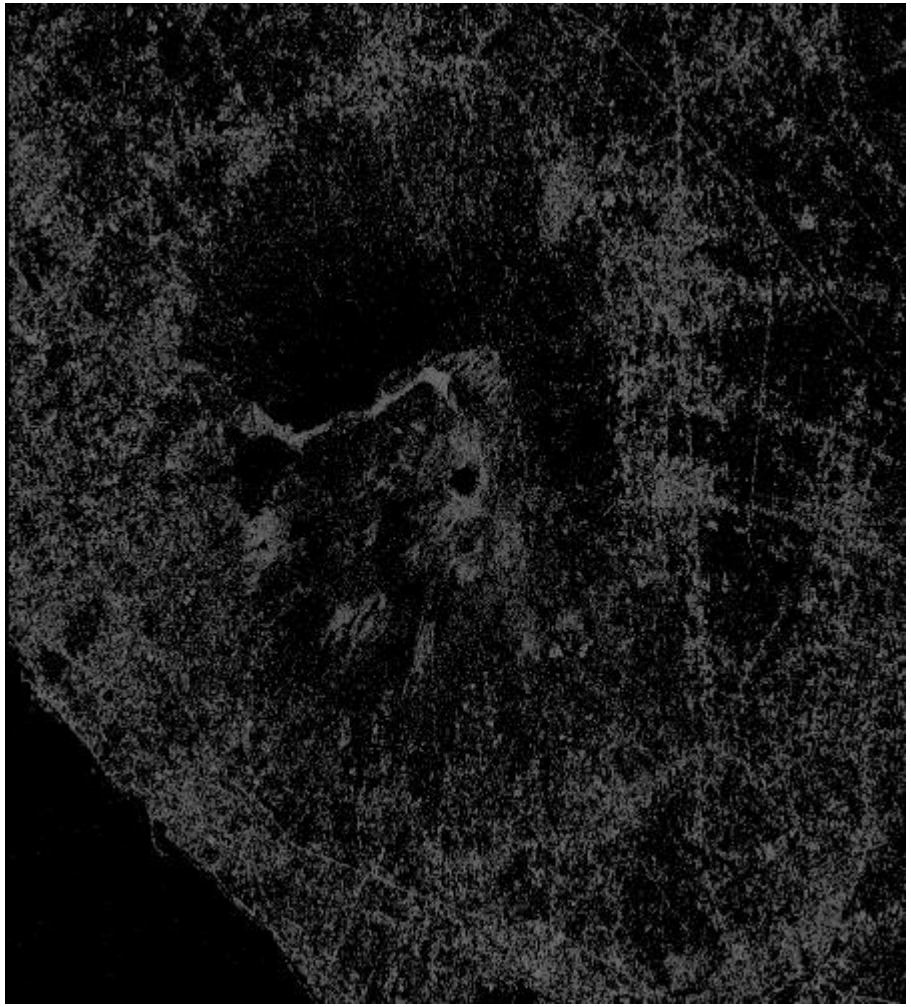

22/08/2017_28/08/2017

Burned Areas: Mt Vesuvius

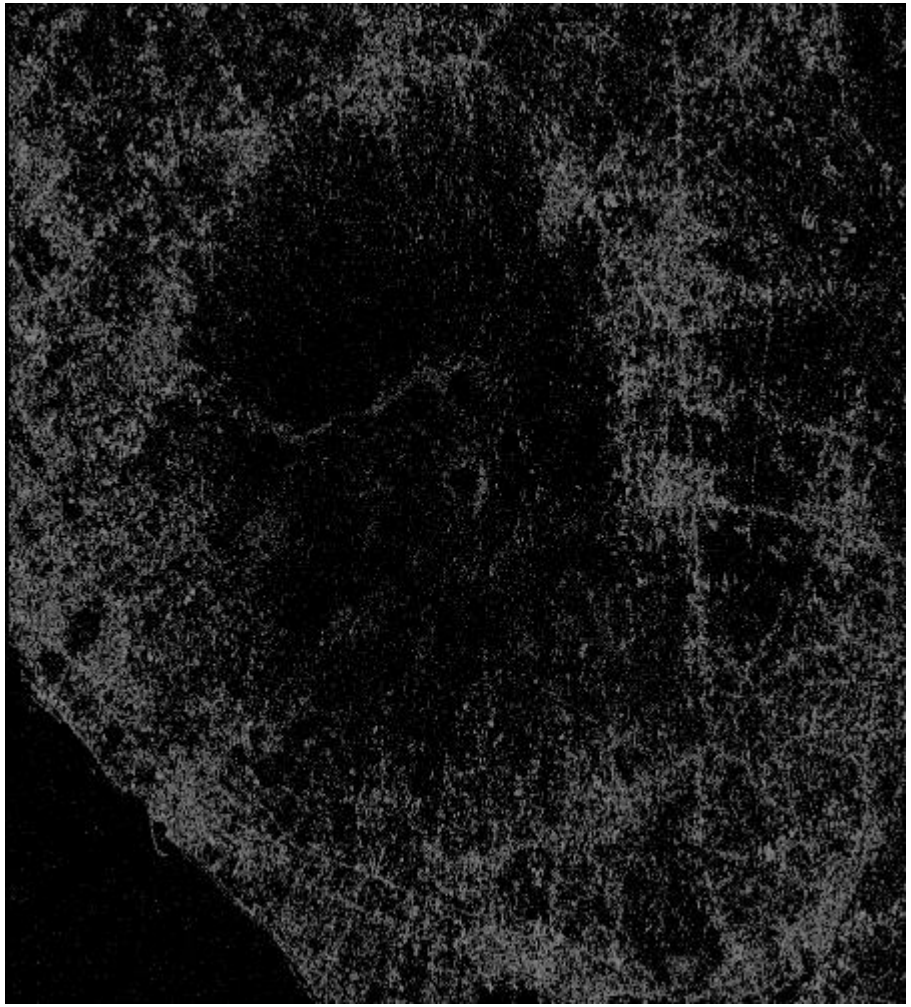

28/08/2017_03/09/2017

Burned Areas: Mt Vesuvius

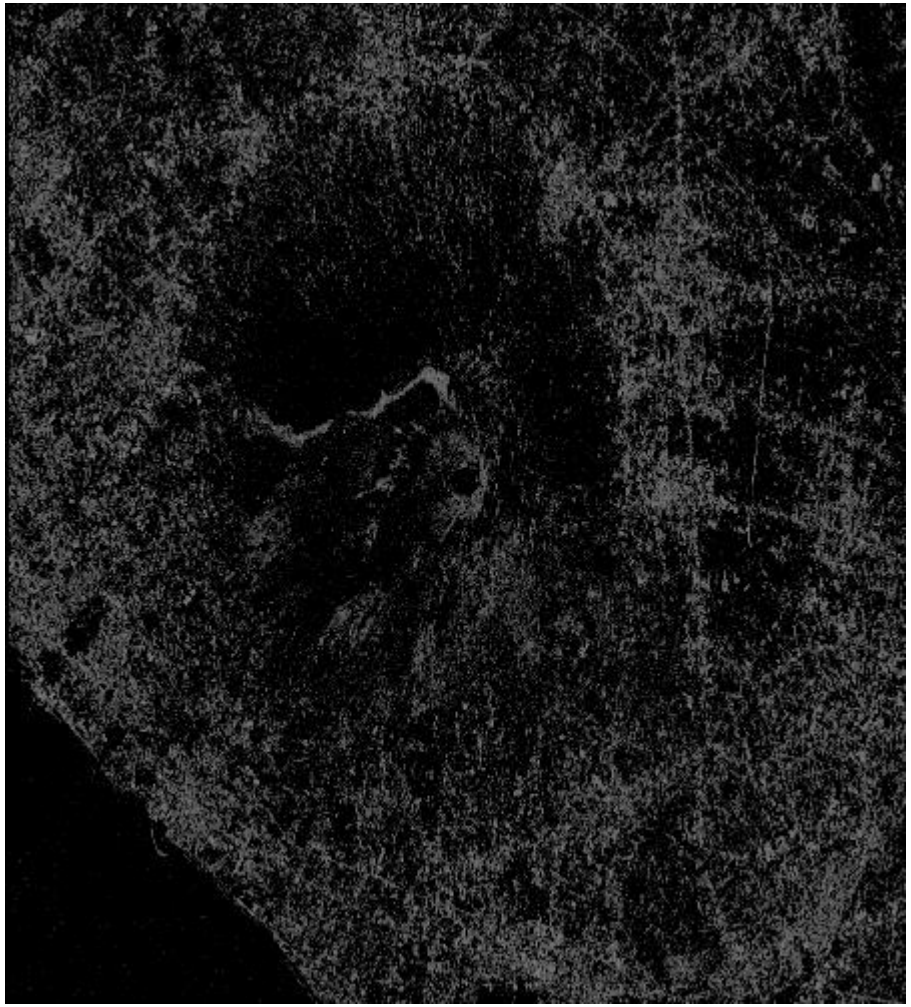

03/09/2017_09/09/2017

Burned Areas: Mt Vesuvius

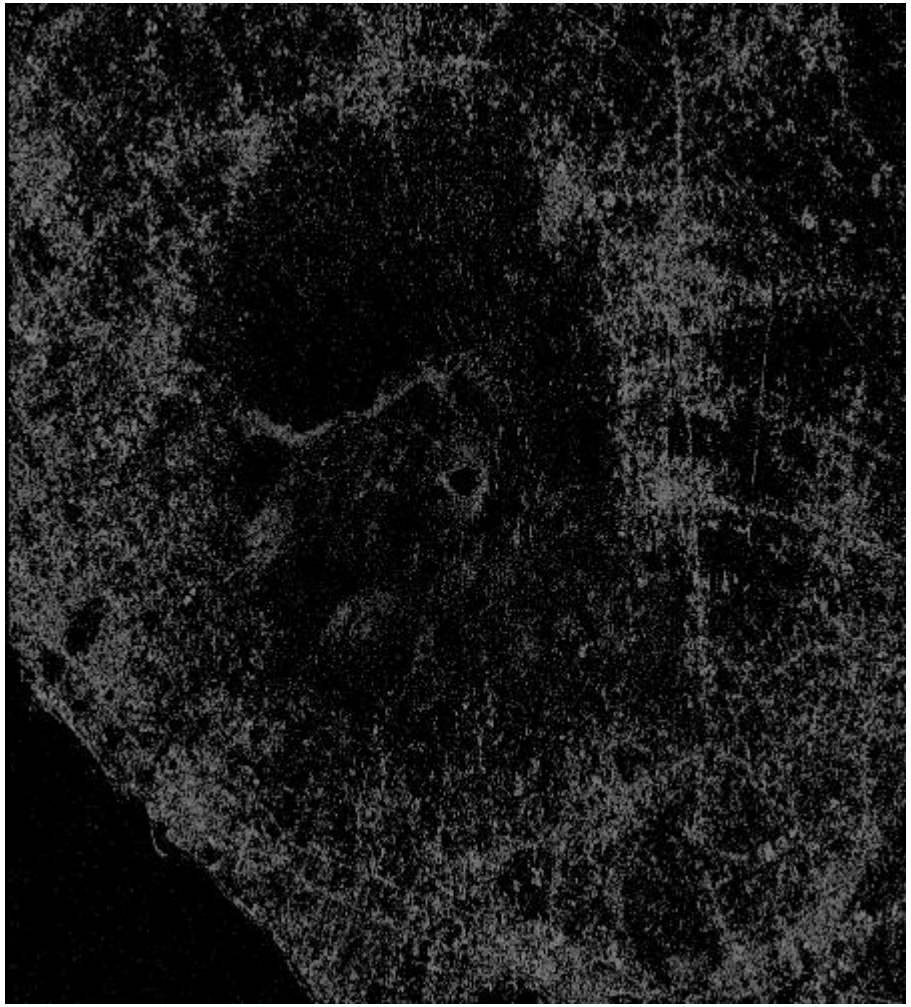

09/09/2017_15/09/2017

Burned Areas: Mt Vesuvius

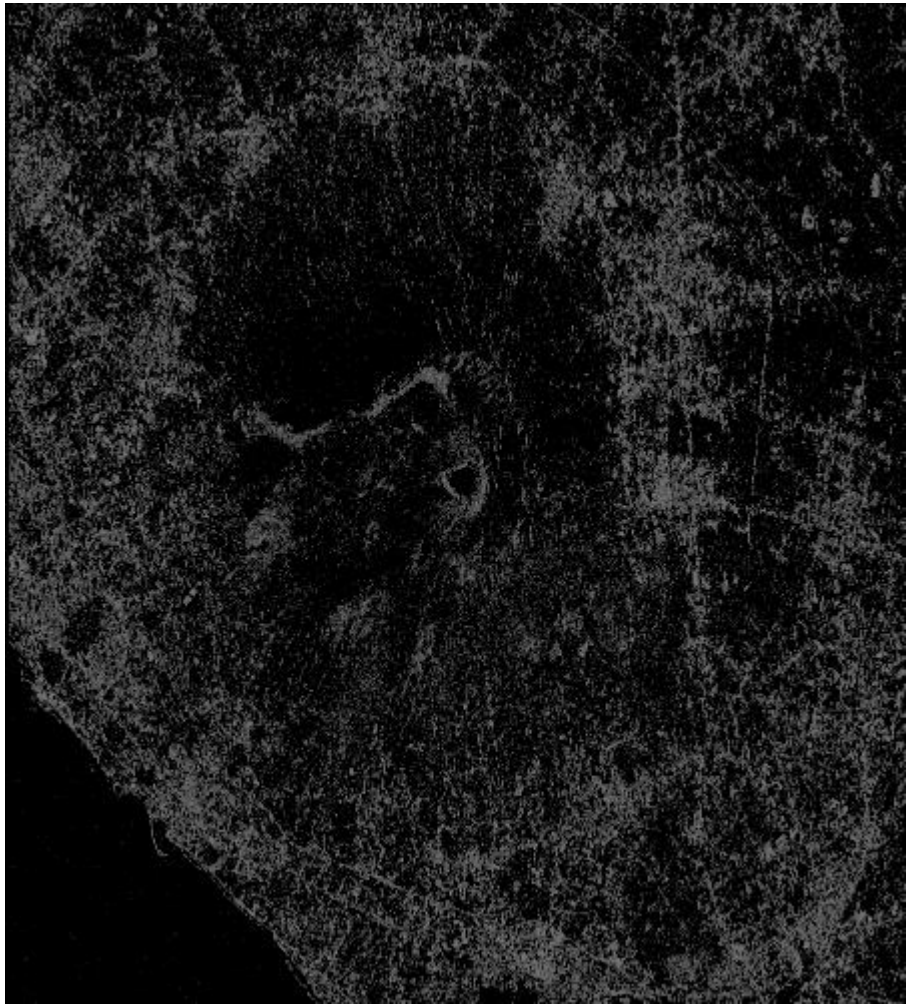

15/09/2017_21/09/2017

Burned Areas: Mt Vesuvius

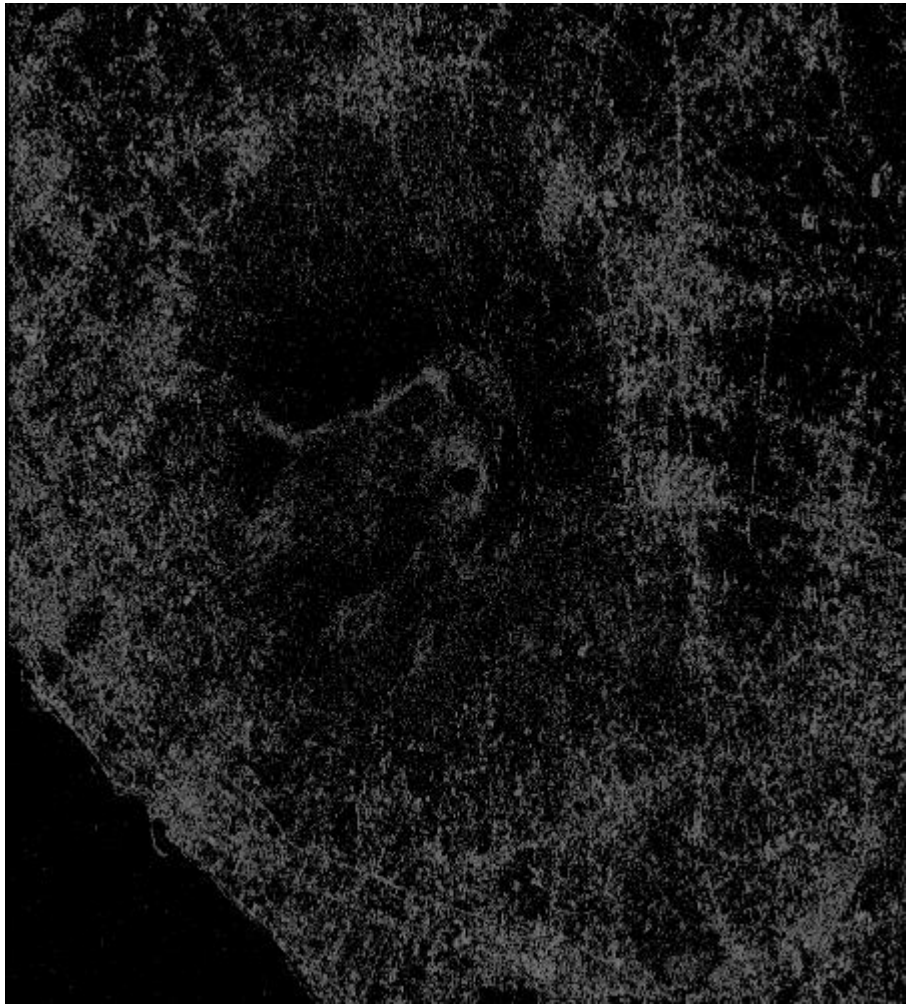

21/09/2017_27/09/2017

Burned Areas: Mt Vesuvius

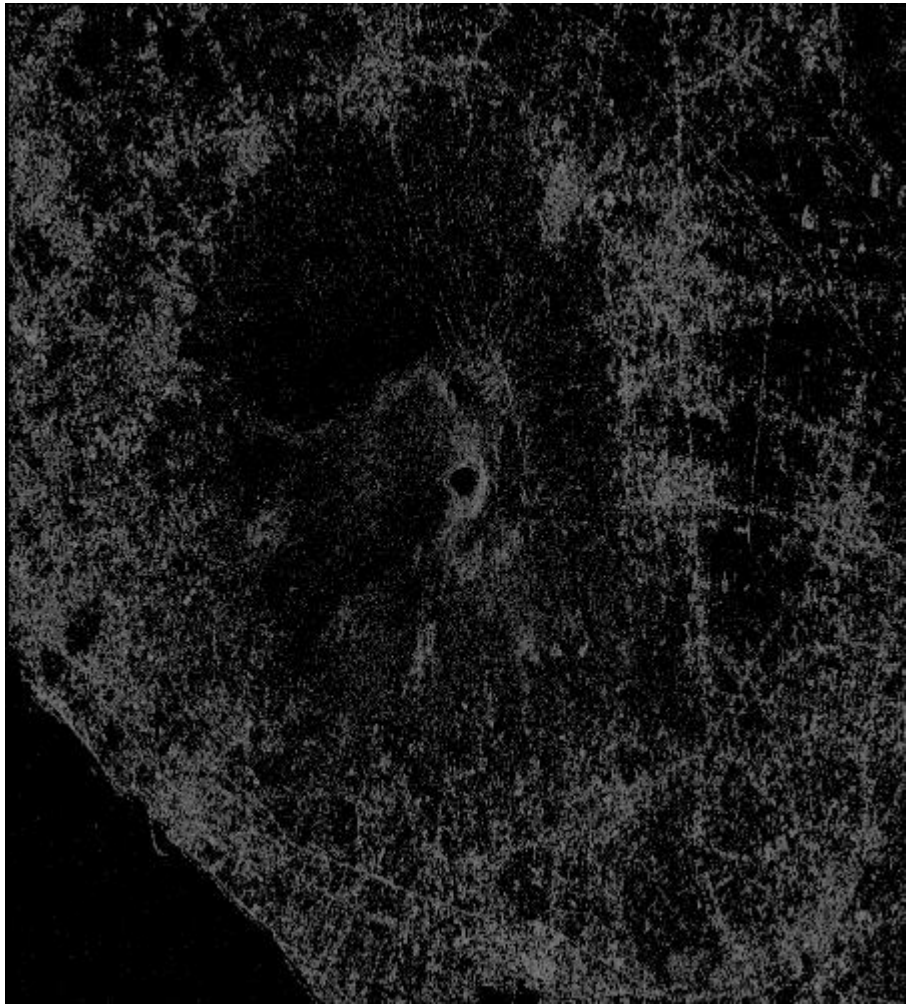

27/09/2017_03/10/2017

Burned Areas: Mt Vesuvius

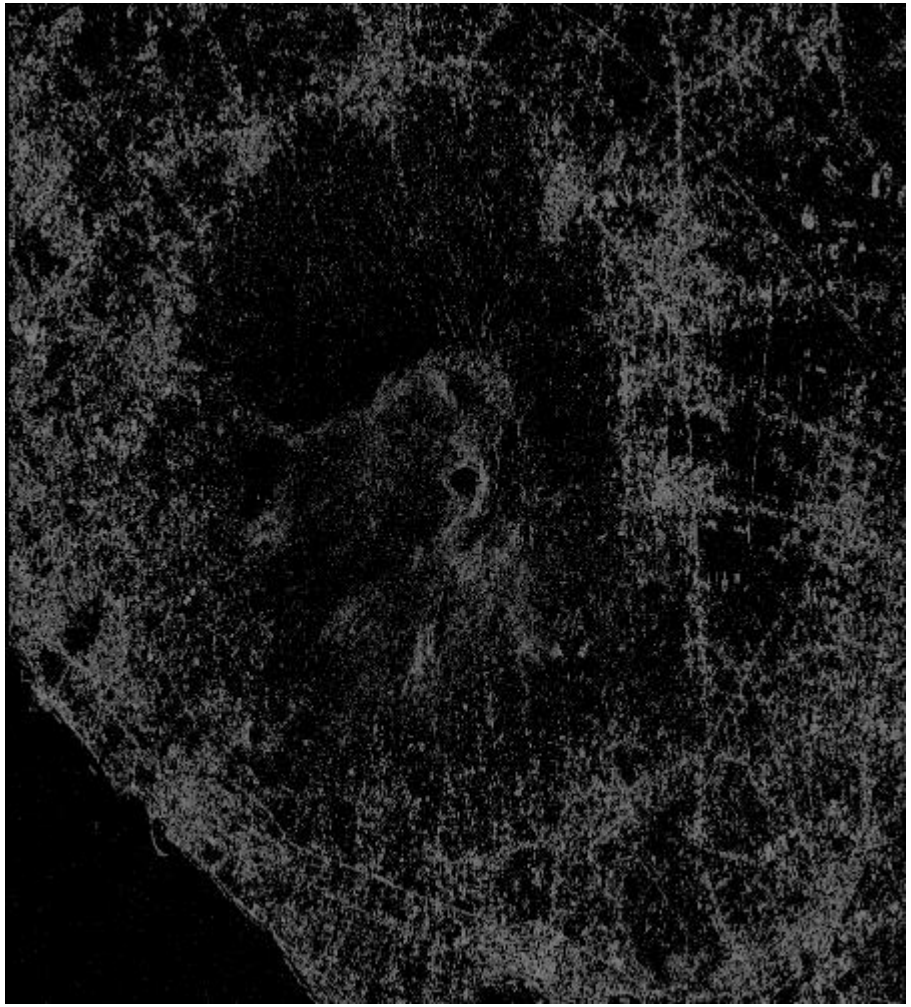

03/10/2017_09/10/2017

Burned Areas Detection

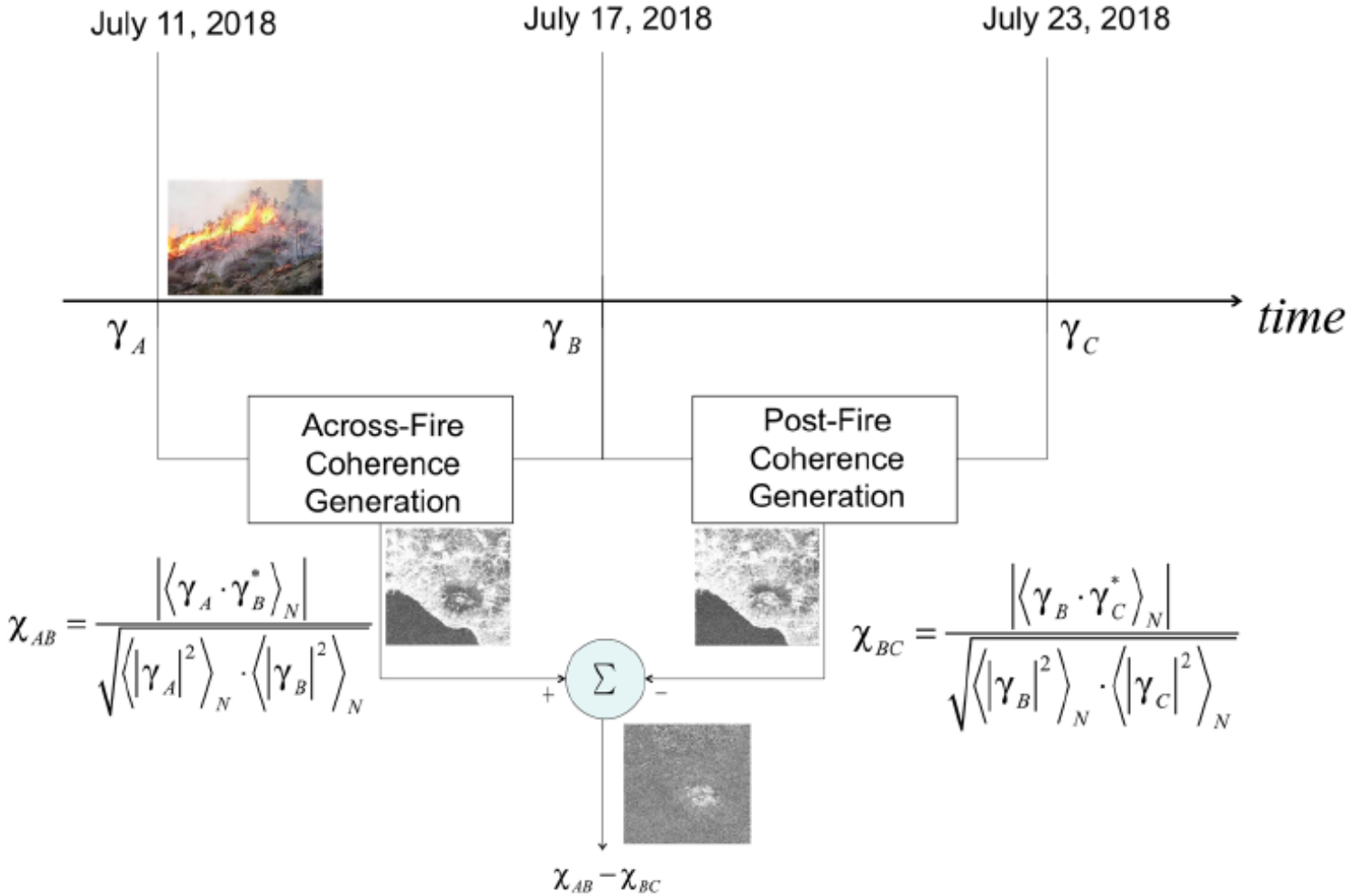

Figura 4. InSAR coherence generation diagram flow. The three complex-valued SLC SAR images γ_A, γ_B, and γ_C are acquired at times t_A, t_B and t_C. Starting from these images, across-fire and a post-fire coherence maps are obtained. The symbol represents the spatial averaging operation with N being the number of used looks.

Burned Areas Detection

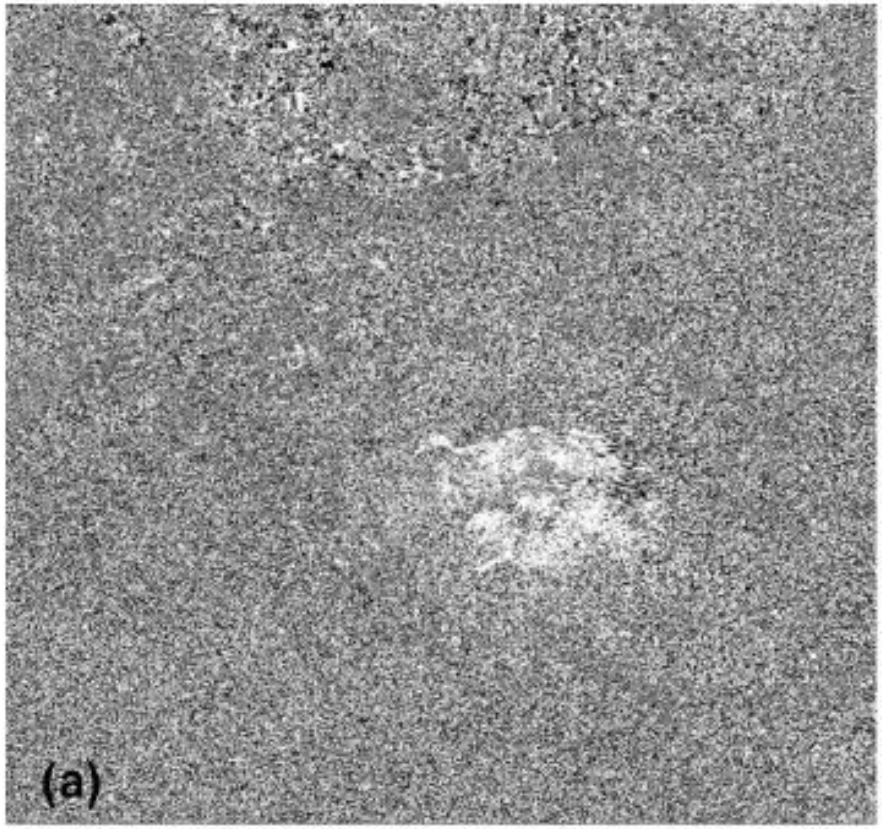

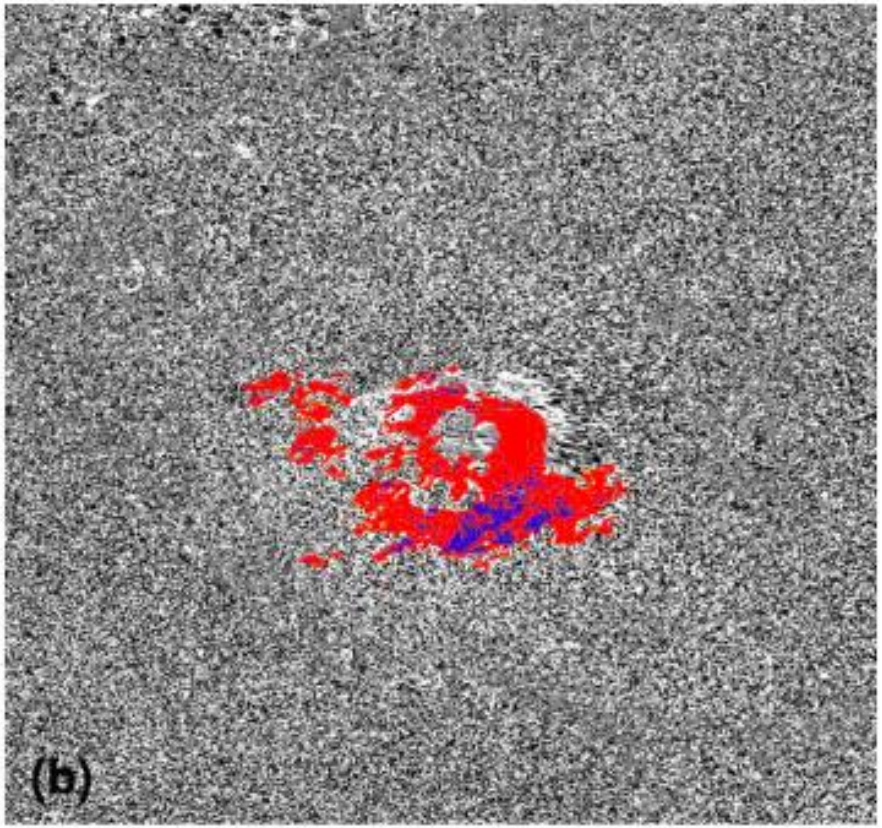

Multi-Pass Coherent Change Detection

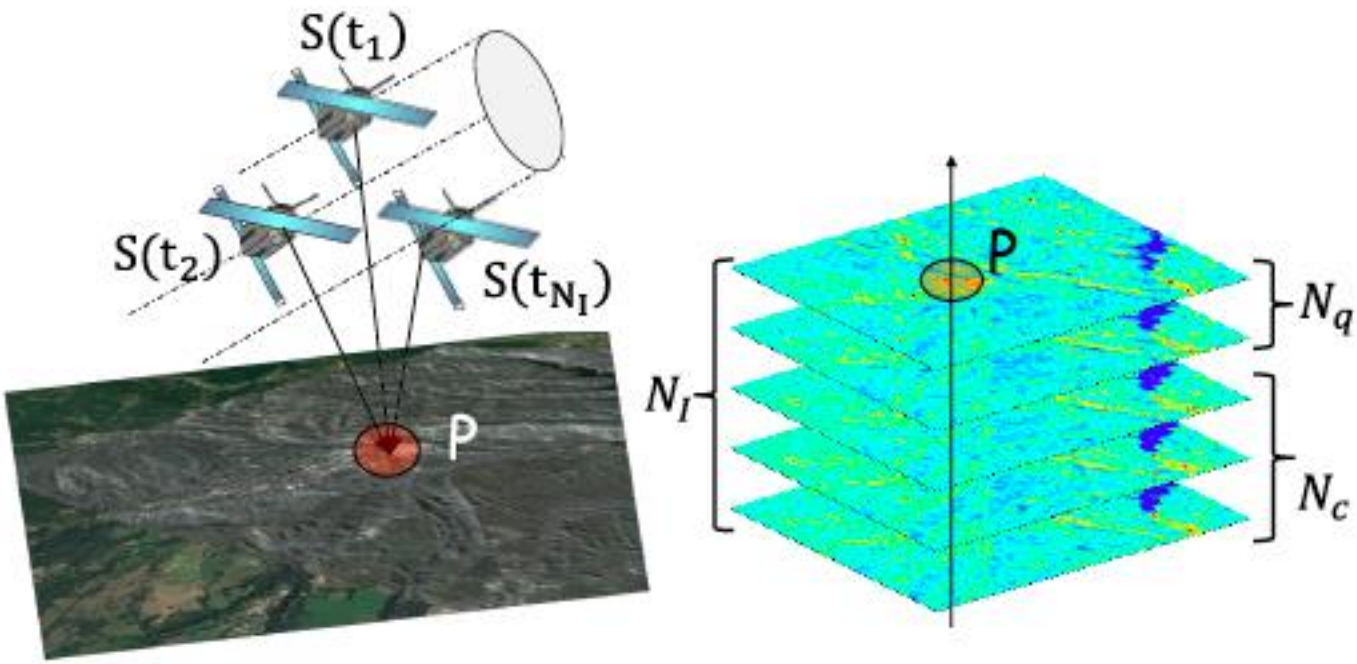

Fig. 1. (Left) Geometry of a multibaseline interferometric SAR, showing the sensor position at different time, and the target under test. (Right) Model of the stack of N_I images, where a change occurred to the target P creates two subsets of N_c and N_q images each.

Andrea Virgilio Monti-Guarnieri , Maria Antonia Brovelli, Marco Manzoni, Mauro Mariotti d'Alessandro, Monia Elisa Molinari, and Daniele Oxoli, "Coherent Change Detection for multipass SAR," IEEE TRANSACTIONS ON GEOSCIENCE AND REMOTE SENSING, VOL. 56, NO. 11, NOVEMBER 2018

GLRT

The GLRT comes out by comparing the logarithms of (3), with some threshold T

$$L_{\mathrm{PC}} = N_q \log\left(\frac{\sigma_c^2}{\sigma_p^2}\right) + \frac{\sum_{i=N_c+1}^{N_I} |x_{\phi p}(i) - b_p|^2}{\sigma_p^2} - \frac{\sum_{i=N_c+1}^{N_I} |x_{\phi p}(i) - b_c|^2}{\sigma_c^2} \underset{H_{N_c}}{\overset{H_0}{\gtrless}} T \quad (7)$$

Multi-Pass Coherent Change Detection

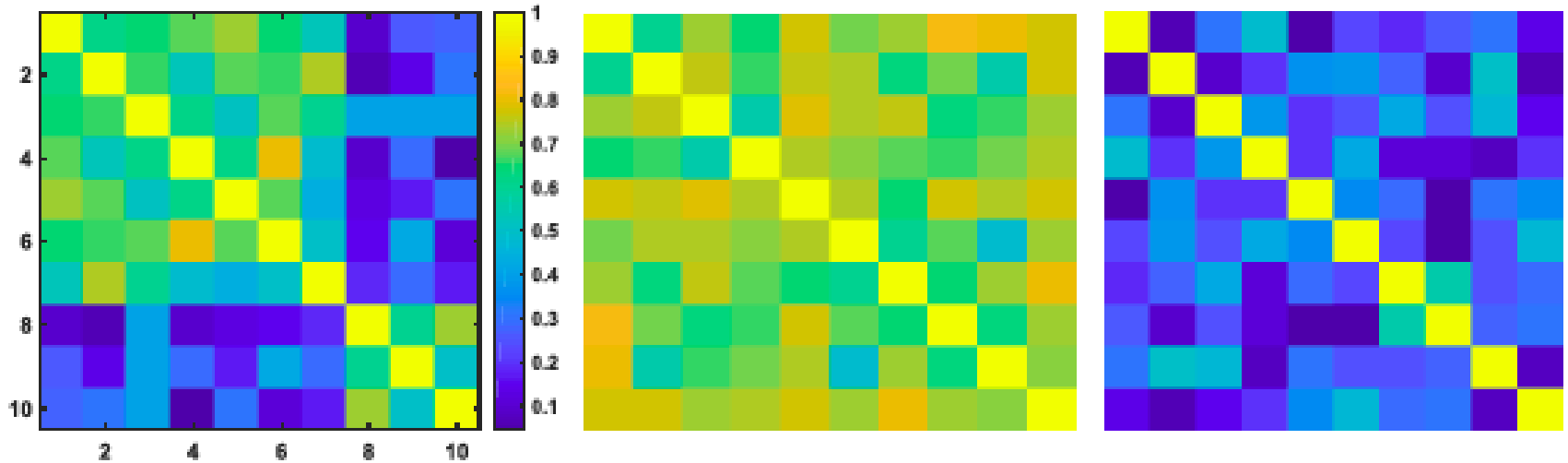

Fig. 9. Coherence matrixes (absolute values) estimated by averaging 10 looks in the case of a change after 7 images (of 10), $\gamma = 0.7$ and of a totally coherent and a totally decorrelated target.

Multi-Pass Coherent Change Detection

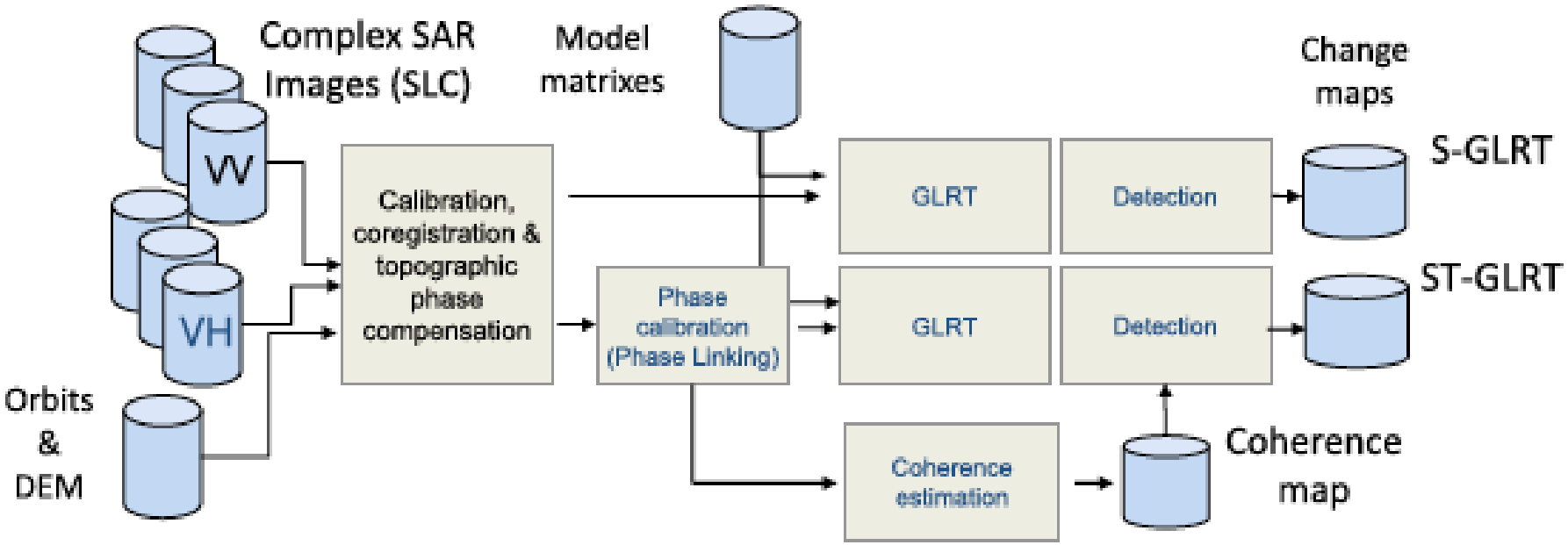

Fig. 7. Schematic of the multipass change detection. The scheme assumes availability of dual-polarized data like for S1 mission.